EU-US Cooperation on Satellite Navigation

Working Group C

COMBINED PERFORMANCES FOR OPEN GPS/GALILEO RECEIVERS

Final version

July 19, 2010

The technical information contained in this note does not represent any official US Government, FAA, EU or EU Member States position or policy. Neither organisation from the US or the EU makes any warranty or guarantee, or promise, expressed or implied concerning the content or accuracy of the views expressed herein.

Executive Summary

The US-EU Agreement on GPS-Galileo Cooperation signed in 2004 laid down the principles for the cooperation activities between the United States of America and the European Union in the field of satellite navigation. In particular, the work undertaken by Working Group A has lead to an interoperable and compatible signal design for the GPS and Galileo systems.

The Agreement also foresaw "a working group to promote cooperation on the design and development of the next generation of civil satellite-based navigation and timing systems", which is the focus of Working Group C.

This note was prepared as part of the Working Group C activities, with the purpose of promoting interoperability of the future GPS and Galileo services by showing the advantages of combining future GPS-III and Galileo open civilian signals. The work presented in this note is intended to serve as a precedent for future analyses on combined performance of different systems and services and to facilitate multilateral discussions in other forums.

In order to be representative of different users, three user receiver types of different complexity were selected for analysis. All three receiver types target the common frequency bands between GPS and Galileo (L1/E1 and L5/E5a). Nominal GPS and Galileo constellations of 24 and 27 satellites respectively were considered. A number of assumptions about signal propagation were made and are described in the note.

Four studies were analysed, covering different user environmental conditions: Principal Study (including urban and open-sky locations), Half Sky Study, Urban Global Study-15º and Urban Global Study-30º.

Accuracy is the main performance indicator chosen for these studies. The accuracy metrics used are daily average position error and in some cases availability of accuracy. These metrics are presented for open-sky and urban environments, and were calculated using both a worldwide grid and the coordinates of population centers exceeding one-half million. Accuracy in different ionospheric activity conditions is also presented.

The studies demonstrate and quantify the improvements that can be expected when using GPS and Galileo open services in combination under different environmental conditions. In all studied cases, the combination of GPS and Galileo led to noteworthy performance improvements as compared to single system performance. The most significant improvement is for partially obscured environments, where buildings, trees or terrain block portions of the sky. The increased number of satellites available provides stable performance even when some signals are blocked, which is reflected in a significant increase of positioning accuracy and availability. The results also confirm that dual-frequency receivers provide an improvement over single-frequency in most environments. Finally, the document highlights the benefit expected from the future broadband signals on GPS L1 and Galileo E1.

This technical note was prepared by the Working Group C with the MITRE Corporation and University FAF Munich as main contributors and with the participation of Stanford University and DLR. The technical activities leading to the results presented in this note were conducted by the MITRE Corporation and University FAF Munich.

TABLE OF CONTENTS

1 INTRODUCTION AND PURPOSE 5
2 ASSUMPTIONS 6
2.1 Receiver Assumptions 6
2.2 Environmental Assumptions 7
2.2.1 Ionosphere 8
2.2.2 Troposphere 9
2.2.3 Multipath 9
2.2.4 Interferences 11
2.3 System Assumptions 11
3 PERFORMANCE 13
3.1 Performance Definition 13
3.2 Process Description 13
3.2.1 Determination of User Sites 13
3.2.2 Calculation of VPE and HPE 14
3.3 Performance Results 14
3.3.1 Principal Study 15
3.3.2 Half Sky Study 16
3.3.3 Urban Global Study - 15° Mask angle 17
3.3.4 Urban Global Study - 30° Mask Angle 17
4 CONCLUSIONS 29

List of Tables

Table 2-1 –Receiver Types 6

Table 2-2 –Traceability between studies and environmental assumptions 7

Table 3-1: Principal Study - Global Statistics of Mean VPE and HPE (m) for Average Solar Cycle 20

Table 3-2: Half-Sky Study - Global Statistics of Mean VPE and HPE for Average Solar Cycle 23

Table 3-3: Urban Global Study (15º) – Global Statistics of Mean HPE and VPE for Peak Solar Cycle 26

Table 3-4: Urban Global Study (30º) – Global Statistics of Mean VPE and HPE for Peak Solar Cycle 28

List of Figures

Figure 2-1 - Open Sky Multipath Models Generated by Mats Brenner's Method.....10

Figure 2-2 - Urban Multipath Errors generated by Jahn Model.....11

Figure 3-1: Principal Study - Comparison of Mean VPE(m) for Average Solar Cycle ..18

Figure 3-2: Principal Study - Comparison of Mean HPE(m) for Average Solar Cycle ...19

Figure 3-3: Principal Study - Empirical CDFs of All Values of VPE and HPE for Average Solar Cycle.....21

Figure 3-4: Half-Sky Study - Comparison of Half Sky Mean HPE(m) for Average Solar Cycle.....22

Figure 3-5: Half Sky Study - Availability of Accuracy (H=12m; V=14m); no satellite failure.....24

Figure 3-6: Urban Global Study (15º) -Comparison of Mean HPE(m) for Peak Solar Cycle.....25

Figure 3-7: Urban Global Study (30º) -Comparison of Mean HPE(m) for Peak Solar Cycle.....27

1 INTRODUCTION AND PURPOSE

Thanks to the degree of interoperability and compatibility achieved already in the definition of GPS and Galileo through the US-EU Cooperation Agreement, GPS and Galileo systems can be easily combined in a satellite navigation receiver by the effective use of the same frequency bands, bandwidths and modulations. The time synchronisation between constellations also assists in this interoperability. This note presents an analysis on the performances that can be obtained by combining GPS and Galileo future constellations for non-aviation open service users. This analysis was performed by Working Group C of the US-EU GPS-Galileo Cooperation Agreement.

The objective of the note is to promote the combined use of GPS and Galileo by showing the performance improvement gained thanks to dual use and the advantages of the system interoperability. The work presented in this note is intended to serve as a precedent for future bilateral analyses on combined performance for other services and systems, and to facilitate multilateral discussions in other forums.

The following sections present an evaluation of the positioning accuracy obtained with GPS, Galileo and combined GPS/Galileo. Results are provided for several generic non-aviation use cases (open sky, urban, half sky) for a number of receivers. Several assumptions were made concerning the receiver characteristics, propagation models and also the GPS and Galileo constellations, and are described in this note.

Section 2 presents the three receiver types considered in the study, the environmental assumptions (ionosphere, troposphere, and multipath) and the GPS and Galileo constellation assumptions. Section 3 defines the performance metrics, describes the process followed to obtain them, and presents the simulation results. Section 4 presents the conclusions. The document is complemented by some appendixes which provide the required background to understand the assumptions and the process followed.

This technical note was prepared by the Working Group C with the MITRE Corporation and University FAF Munich as main contributors and with the participation of Stanford University and DLR. The technical activities leading to the results presented in this note were conducted by the MITRE Corporation and University FAF Munich.

2 ASSUMPTIONS

This section presents the assumptions used in the note for the receiver types (frequency bands, bandwidths, noise, tracking loop discriminator), signal propagation (ionospheric, tropospheric, and multipath errors) and GPS and Galileo systems (constellation, clock and ephemeris errors and inter-system synchronisation).

2.1 Receiver Assumptions

With the purpose of being representative of many different users, three receiver types were defined, each one able to process a different set of signals from GPS-III and Galileo.

Receiver type	*Frequency Mode*	*Processed Signals*	*Modulations*	*Bands and Bandwidths*
SF BOC(1,1)	Single Frequency	GPS L1C, Galileo E1	BOC(1,1)	1575.42 MHz ± 2 MHz
SF MBOC	Single Frequency	GPS L1C, Galileo E1	MBOC	1575.42 MHz ± 7 MHz
DF	Dual Frequency	GPS L1C + L5, Galileo E1 + E5a	MBOC - BPSK-R(10)	1575.42 MHz ± 7 MHz 1176.45 MHz ± 10 MHz

Table 2-1 –Receiver Types

The first receiver type (SF BOC(1,1)) represents the simplest GPS/Galileo receiver architecture. This receiver type would minimise cost and power consumption and therefore could be used for a number of mass market applications in the early days of combined GPS/Galileo service introduction.

The second receiver type (SF MBOC) proposes a broader bandwidth with respect to the first one to support the MBOC signals (GPS-III TMBOC [13] and Galileo CBOC [17]). This receiver type may imply a small increase in complexity and power consumption but also is expected to deliver better performances in most environments and applications.

The third receiver type (DF) includes a second frequency band in L5/E5a in addition to the L1/E1 band in the receiver described above. This receiver type would imply a step forward in accuracy due to the ionosphere error correction but also higher complexity and power consumption. For simplicity reasons, only the Galileo E5a and GPS L5 signals were considered in the study, although the combination of GPS L5 and the broader Galileo E5ab AltBOC signal may be also interesting for future users.

A perfect carrier and loop tracking was assumed, so that the receiver thermal noise contribution is equal to zero meters. Since the objective of the work is to demonstrate the relative improvement of combined GPS/Galileo, this assumption does not invalidate the results obtained.

For the multipath error contribution, a non-coherent dot-product discriminator was assumed, with an Early minus Late correlator spacing of 0.1 chips. For details concerning the discriminator function, refer to Appendix A.

A masking angle of 5 degrees of elevation was used by default in the receiver. However, this is only applicable for the Open Sky case, since in the Urban case, no signals are received below 15 degrees of elevation according to the multipath model used.

2.2 Environmental Assumptions

Four different studies were conducted: Principal (including urban and open-sky environments), Half-sky, Urban global-15º and Urban global-30º, with the purpose of showing the combined GPS and Galileo performance in different cases relevant for non-aviation users. These studies are explained in detail in Section 3, but they are associated to certain environmental assumptions which are described in this section concerning ionosphere, troposphere, multipath and interference. Whereas troposphere and interferences are considered the same in all environments, several multipath and ionospheric conditions are studied, depending on the local environmental conditions and the solar activity respectively.

The table below shows the correspondence between the studies and the environmental assumptions for multipath and ionospheric conditions. The table also includes the receiver types considered and the dual frequency combination used in the receiver. The dual frequency combination is different depending on the environmental conditions, as explained later in the note. The following subsections explain and justify the models used.

Study	**Principal Study *Urban***	**Principal Study *Open Sky***	**Half-Sky**	**Urban Global 15º**	**Urban Global 30º**
Ionospheric Activity	Maximum Average Minimum	Maximum Average Minimum	Average	Maximum	Maximum
Multipath model	Jahn	Mats Brenner	Mats Brenner	Jahn	Jahn
Receiver types studied	SF BOC(1,1) SF MBOC DF (WLS iono combination)	SF BOC(1,1) SF MBOC DF (iono-free combination)	SF BOC(1,1) SF MBOC DF (iono-free combination)	SF BOC(1,1) SF MBOC DF (WLS iono combination)	SF BOC(1,1) SF MBOC DF (WLS iono combination)

Table 2-2 –Traceability between studies and environmental assumptions

2.2.1 Ionosphere

Due to the impact of frequency diversity in the ionospheric error contribution in the case of the Dual-Frequency receiver, ionospheric assumptions are separated into two subsections, one for Single-Frequency receivers and the other for the Dual-Frequency receiver.

2.2.1.1 Ionosphere for Single-Frequency Receivers

The single-frequency ionospheric correction model [15] is used to determine the ionospheric error variance for minimum, average, and peak periods of the solar cycle. Since this model predicts the total slant ionospheric delay, scale factors are used to reduce the slant ionospheric delay produced by the model to an ionospheric residual error after applying the Klobuchar model correction in the case of Single-Frequency receivers. In addition, a partial correlation of the ionosphere is applied as shown in Appendix C.

The scale factors and correlation coefficients are different for each solar period. These factors were determined by a validation study described in Appendix E.

While the Galileo system may use a different model for the single frequency ionospheric corrections (NeQuick), that may provide slightly different performances than the simpler Klobuchar method used in GPS, as shown in [18], the approach described above was considered sufficiently representative for both GPS and Galileo and was used for simplicity reasons.

2.2.1.2 Ionosphere for the Dual-Frequency Receiver

Dual-frequency receivers have as their major advantage the ability to eliminate ionospheric delay in the determination of position. The calculation of range error variance includes only three components: (1.) user range error (URE), (2.) tropospheric variance, and (3.) an iono-free variance. For a dual-frequency receiver, the iono-free variance is as follows: (Appendix D)

$$\sigma^2_{iono-free} = \left(\frac{f_1^2}{f_1^2 - f_5^2}\right)^2 \sigma^2_{L1,air} + \left(\frac{f_5^2}{f_1^2 - f_5^2}\right)^2 \sigma^2_{L5,air} = \left(2.26\sigma_{L1,air}\right)^2 + \left(1.26\sigma_{L5,air}\right)^2 \quad (2.1)$$

with $f_1 = 1575.42$ MHz, $f_5 = 1176.45$ MHz

The variances $\sigma^2_{L1,air}$ and $\sigma^2_{L5,air}$ consist of components from thermal noise and multipath. Since thermal noise is considered zero in this study, the entire component originates with multipath. It is immediately obvious from Equation 2.1 that there is a significant multiplying effect in determining the iono-free variance. In an open sky environment where multipath is minimal, this expansion effect is minor and the superiority of dual-frequency receivers over single-frequency receivers is clear. However, in an urban environment there can be very significant multipath for elevation angles below 45° as can be seen in Appendix A. For low elevation angles in the urban environment, the expansion effect shown in Equation 2.1 can be so significant that the innate superiority of dual frequency receivers is lost. It was assumed that dual-frequency receiver manufacturers whose equipment needs to operate in high multipath environments would

likely employ multipath mitigation efforts. In order to account for these environments, the modelling of dual-frequency receivers utilizes a two-tiered approach:

1. For open sky environments where multipath is small, the dual frequency range error uses the iono-free variance of Equation 2.1,

2. For urban environments where multipath can be quite high, the dual-frequency range error uses a weighted least squares combination of L1/E1 MBOC and L5/E5a BPSK-R(10) as shown in Appendix D and [10]. This approach is suggestive of mitigation efforts which could easily be employed in today's receiver technologies.

2.2.2 Troposphere

The tropospheric zenith error is assumed to be 0.05 meters and the mapping function used is presented in Appendix D and also in Appendix A of WAAS MOPS [1]. This residual error is compatible with the implementation of a local prediction model in the user receiver algorithms not necessitating availability of local weather data.

2.2.3 Multipath

Multipath is one of the main contributors to the user position error, especially in environments surrounded by buildings or other obstacles. A thorough characterisation of the user local conditions is outside the scope of this study. Nevertheless, an effort was made to use and validate generally accepted multipath models for user environments. Finally, the Mats Brenner model [12] was used for the Open Sky environment, and the Jahn model [6] for the Urban environment.

The process employed in computing the multipath error contribution to the total user equivalent range error is described in detail in Appendix A. As an outcome of the multipath modelling activity, the multipath parameters and functions chosen are described below.

2.2.3.1 Open Sky: Mats Brenner Multipath Model

This model produces multipath error versus elevation angle for the different signals in the Open Sky environment as shown in Figure 2-1.

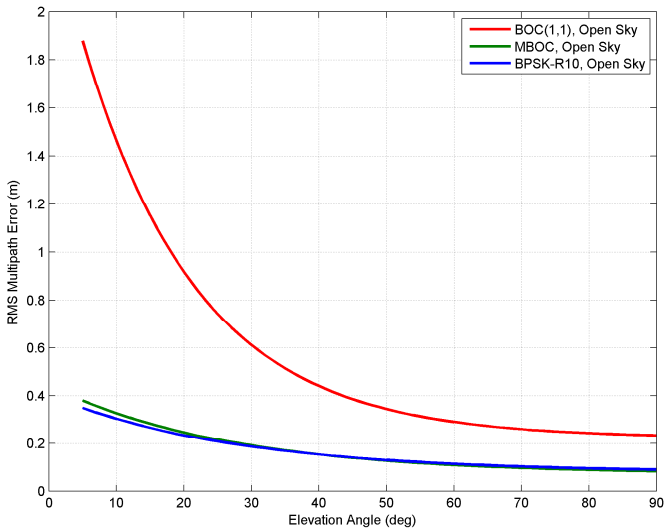

Figure 2-1 - Open Sky Multipath Models Generated by Mats Brenner's Method

The following exponential function was used for the fitting of the 1-sigma multipath error:

$$s\left(meters\right) = a + b \cdot \exp\left(cE\left(\deg\right)\right) \tag{2.2}$$

where *E(deg)* is the satellite elevation in degrees and the parameters *a*, *b* and *c* are listed for each signal in Table A-7 of Appendix A.

2.2.3.2 Urban: Jahn Multipath Model

In a similar manner, the Jahn model was implemented for the urban environment, as in other previous performance studies like [19]. Using the RMS values obtained from the multipath simulations, the curves represented in Figure 2-2 were generated.

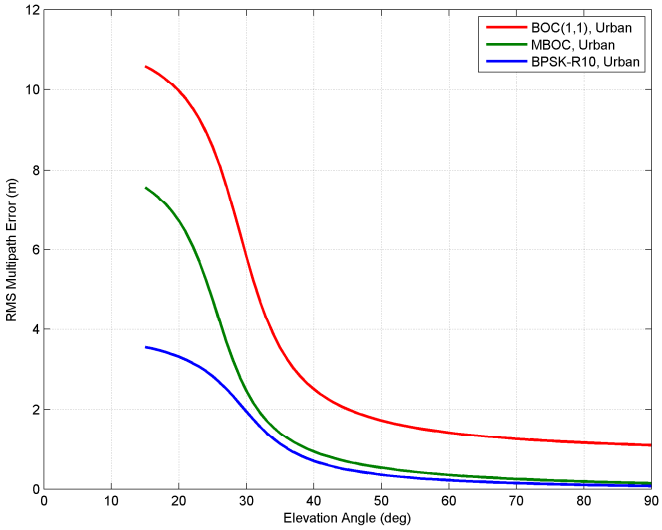

Figure 2-2 - Urban Multipath Errors generated by Jahn Model

The following arc-tangent function was used for the fitting of the 1-sigma multipath error:

$$\mathrm{s}\left(meters\right) = a + b \cdot \mathrm{atan}\left(c\left(E\left(\mathrm{deg}\right) - d\right)\right) \qquad (2.3)$$

where *E(deg)* is the satellite elevation in degrees and the parameters *a*, *b*, *c* and *d* are listed for each signal in Table A-4 of Appendix A.

2.2.4 Interferences

All simulations were carried out assuming that there are no interfering signals.

2.3 System Assumptions

The GPS constellation considered is a 24-slot constellation based on the GPS almanacs provided in GPS SPS [14], with the Right Ascension of Ascending Node (RAAN) = OMEGA_0 + GMST (at July, 1, 1993, 0, 0, 0).

A Galileo nominal constellation definition of 27 satellites (Walker 27/3/1) was used. Both constellations synchronised for July 1st 1993 00:00:00.

Appendix B provides the almanac tables with the GPS and Galileo constellation definitions used.

No satellite failures were considered for the analysis. Instead, results are presented for all-in-view for open sky, half sky and urban environments.

The following standard deviations of the satellite ephemeris and clock error distributions, referred also as user range errors or UREs, were considered:

$$s_{clk\_eph,Gal} = 0.7\text{m} \quad (2.4)$$

$$s_{clk\_eph,GPS} = 0.25\text{m} \quad (2.5)$$

The Galileo URE value used at this stage corresponds to a design assumption and includes margins that are expected to be reduced in the future, once system verification activities have established the actual performance based on field measurements.

In order to combine GPS and Galileo at a user position, the measurements from the two systems must be synchronised to a common time reference. To achieve a common time reference, it was assumed that the broadcast GPS Galileo Time Offset (GGTO) parameter is used in the positioning equation. The following GGTO error was considered:

$$s_{GGTO} = 2.5\text{ns} \text{ (equivalent to } 0.7495\text{m)} \quad (2.6)$$

Appendix C presents the equations used for the calculation of a combined GPS/Galileo position solution. If a broadcast GGTO is not used, then an additional unknown must be solved in the positioning equations and a minimum of five satellites are needed to compute the position solution.

The effect of the differences in the reference frames used by GPS (WGS84) and Galileo (GTRF) were considered negligible for the purpose of the study.

3 PERFORMANCE

The criterion chosen to illustrate the benefits of a combined GPS/Galileo constellation is accuracy obtained by non-aviation users. Increased performance based on accuracy where no safety-of-life considerations need be considered can yield the widest possible benefits.

3.1 Performance Definition

The metrics used to measure accuracy are vertical position error (VPE), horizontal position error (HPE), and availability. VPE and HPE are calculated as shown in section 3.2.2. Availability is the probability (equivalent to the expected fraction of time) that VPE and HPE are within required limits. Since there are currently no requirements for these limits, availability is not generally used in this report. Instead, measures of VPE and HPE were determined to directly assess performance for each of the three constellations studied: GPS, Galileo, and combined GPS/Galileo. The three receivers relevant to this study (single-frequency (SF) BOC(1,1), SF MBOC, and dual-frequency (DF) MBOC-BPSK-R(10)) have VPE/HPE metrics determined for them separately to distinguish their performance and show the effects of the ionosphere on single frequency operations during the solar cycle.

Relative performance information was organised in three ways:

1. Charts of daily average VPE and HPE determined at every user site throughout the world representing all combinations of the three constellations and three receivers studied. To show the effects of the ionosphere, these charts were produced for minimum, average, and peak solar cycle conditions.

2. Tables of statistics of site-derived mean VPEs and HPEs for each combination of constellation and receiver.

3. Empirical cumulative distribution functions (CDFs) for all values of VPE and HPE determined throughout the day.

3.2 Process Description

3.2.1 Determination of User Sites

At each user site throughout the world, VPE and HPE were calculated at 5 minute epochs using all satellites visible to that user. Sites were divided into two classes: (1.) *open sky* points which are distributed uniformly over the surface of the Earth, and (2.) *urban* points representing all population centers exceeding one-half million.

Open Sky points were calculated to be regularly separated in longitude and latitude. This technique prevents over sampling at polar latitudes which occurs with a standard grid. To determine this regular grid, points were sampled every three degrees in latitude from the Equator to the North and South Poles. Each latitude circle created has points separated in longitude as described in [1].

Every open sky point employed the Mats Brenner multipath model (as described in Appendix A) and a mask angle of 5 degrees in the process of determining its error variance [2], [3]. There are 4586 open sky points.

Population data was obtained from the Center for International Earth Science Information Network (CIESIN) of the Earth Institute at Columbia University [16]. Cities with populations exceeding one-half million were selected. All urban sites employed a mask angle of 15 degrees and the Axel Jahn multipath models [6] as described in Appendix A. There are 587 population sites.

There are a total of 5173 sites and separate statistics were produced for open sky and urban sites.

3.2.2 Calculation of VPE and HPE

VPE and HPE are the vertical and horizontal position error components defined as follows:

$$\begin{aligned} VPE &= 2d_V \\ HPE &= 2d_{rms} = 2\sqrt{d_{\text{major}}^2 + d_{\text{minor}}^2} \end{aligned} \tag{3.1}$$

with d_{major} and d_{minor} the semi-major and semi-minor axes of the horizontal error ellipse. The d_{minor} axis can assume values in the range [0 d_{major}] where respectively the error ellipse ranges from a straight line to a circle. If each of the error components in the east, north, and vertical directions is assumed to be normally distributed with zero mean, then the probability associated with VPE is 0.9545 and the probability associated with HPE ranges from 0.9545 to 0.982 as the error ellipse extends from a straight line to a circle [11].

VPE and HPE are calculated using a weighted least-squares solution as follows:

$$\begin{aligned} VPE &= 2\sqrt{C_{3,3}} \\ HPE &= 2\sqrt{C_{1,1} + C_{2,2}} \end{aligned} \tag{3.2}$$

where the covariance matrix $C = (G^T W G)^{-1}$ with G the observation matrix and W the weighting matrix as shown in Appendix C. W is comprised of weights formed by the range error variances. These total variances are a combination of individual variances from user range errors (URE), tropospheric errors, ionospheric errors, and multipath errors as shown in Appendix D.

3.3 Performance Results

Performance results were presented in the form of studies made to examine the effects of a combined constellation given certain conditions and assumptions. Four studies were performed:

1. *Principal Study:* Effects on VPE and HPE arising from different constellations, receivers, and solar cycle periods.

2. *Half Sky Study:* Effects on VPE and HPE and availability arising from different constellations and receivers, the average solar cycle period, and a partially occluded sky which eliminates satellites with azimuths between 0 and 180 degrees. The other side of the sky is clear and is considered open sky. This study simulates the effects of being on the western side of a building where everything to the East is blocked, but everything to the West is open. Only uniformly distributed user sites were used in this study.

3. *Urban Global Study (15° mask angle):* Effects on VPE and HPE for single and dual frequency receivers arising from different constellations, the peak solar period, and all sites in the world considered urban. Only uniformly distributed user sites were used in this study.

4. *Urban Global Study (30° mask angle):* Study 3 with the application of a 30° mask angle. This study shows the effects of masking out low elevation angles which incur the highest multipath in an urban environment.

The following sections present some insight on the interpretation of the results for the four studies and highlight the aspects considered most relevant. The figures and tables with the performance results are provided just afterwards.

3.3.1 Principal Study

All of the results of the principal study for minimum, average, and peak solar periods are presented in Appendix F. This section presents the results for the average solar cycle. A restriction on Position Dilution of Precision (PDOP) was imposed so that the results occur only when PDOP is lower or equal to 10. For this simulation, that restriction has almost no effect. Results are presented according to the three performance measures listed in Section 3.1: world charts of mean VPE/HPE, tables of statistics on mean VPE/HPE, and empirical CDFs of all values of VPE/HPE. These results are depicted for all constellations and receivers. For each user, the VPE and HPE are calculated for each time epoch using all satellites visible to that user. The average VPE and HPE are calculated over 288 epochs at each user. The 95th percentiles of mean values are calculated for open sky and urban points separately and appear in the lower right text boxes for each map. The sites with the highest values of VPE/HPE tend to be the urban areas.

Figure 3-1 shows a VPE reduction due to the GPS and Galileo combination which is quite evident in the Urban case. For example, in the SF BOC(1,1) case, VPE (mean, 95%) is reduced from 20-22 meters to 12.8 meters, that is, a reduction of more than 40%. For the Open Sky case there is an improvement, but the improvement is not so evident given that DOP values are already low for each constellation. However, improvements in the order of 1 to 2 meters are still visible. Mean VPEs and HPEs tend to be larger around the geomagnetic equator in Open Sky SF cases due to the predominance of ionospheric error, which is not observable in the DF Open Sky case.

The improvements of MBOC versus BOC(1,1) are more significant in the Urban case, given that multipath is the dominant source of error and it is significantly reduced due to the MBOC signal. It should be noted, however, that some high-sensitivity receivers in severe multipath conditions may increase availability at the expense of accuracy by using signals for which only reflections are received, in which case the advantage of the

MBOC with respect to BOC(1,1) may not be directly translated in a better position solution.

As expected, the use of the DF iono-free combination in the Open Sky environment reduces positioning error by several meters. This improvement is not so evident in the Urban Environment for the reasons explained below for Figure 3-3, yet it yields slightly better performance than the SF MBOC case.

Figure 3-2 shows a similar trend for HPE as Figure 3-1 for VPE. HPE is in general lower than VPE due to satellite geometry.

Table 3-1 shows the global statistics on the *means* of VPEs and HPEs determined at each site for open sky and urban environments. It can be noticed that the availability for each constellation (PDOP at least 10 and at least 4 satellites) appears as more than 99% for the Urban case, which may not be achievable in severe urban conditions. This issue is further analysed in the Half Sky study and Urban Global 30º study presented below.

Finally, Figure 3-3 shows the empirical CDFs for *all* values of VPE and HPE calculated during the day (not the daily means). They show similar performance of BOC(1,1) and MBOC for the Open Sky case and a major improvement of MBOC versus BOC(1,1) in the Urban case, as observed in the previous figures. It should be noted that part of the HPE CDFs of SF MBOC are to the left of the dual frequency CDF. This is due to the fact that partial correlation between satellites is assumed for single frequency receivers and not for dual frequency receivers in this study. As explained before, a weighted least squares combination of L1/E1 MBOC and L5/E5a BPSK-R(10) was used for the urban case.

3.3.2 Half Sky Study

The half sky study was proposed as a view into the effects of partial sky occlusion that might arise in an urban area. All satellites from 0 to 180 degrees azimuth are excluded. The satellites to the West are not blocked and that view is considered open sky. The simulation presents a global view of the effect, so only the regularly distributed open sky points are used. One solar cycle period, average, was selected. A restriction on PDOP was imposed so that the results occur only when PDOP is at least 10 and there are at least 4 satellites in view.

Results are depicted for all constellations and receivers. For each user, VPE and HPE are calculated for each time epoch using all satellites visible to that user. The average VPE and HPE are calculated over 288 epochs at each open sky site. Given that the focus of the study is non-aviation users and the VPE and HPE results follow the same trends, only HPE plots are presented in the core part of this study (Figure 3-4). Global statistics are available for both HPE and VPE (Table 3-2). All the remaining plots (VPE, CDFs) can be found in Appendix F.

Figure 3-4 shows a significant improvement in accuracy thanks to dual GPS/Galileo use, e.g. from 12.59m and 14.17m for GPS and Galileo respectively to 8.34m for dual case, SF BOC(1,1). The improvement from BOC(1,1) to MBOC is not so relevant as in the Urban case of the Principal Study, due to the dominant contribution of poor geometry and ionosphere over multipath, given that the Open Sky multipath model is used.

Figure 3-4 does not provide availability metrics and therefore the accuracy information may be incomplete. The significant improvement in position availability can be seen in Table 3-2 statistics: from 63.16% and 78.57% for GPS and Galileo respectively, with nominal constellations of 24 and 27 satellites each, up to 98.92% for the dual case.

To illustrate the dramatic improvement in availability by combining GPS and Galileo, an availability of accuracy chart is also presented in Figure 3-5. Horizontal and vertical accuracy requirements of 12m and 14m respectively are derived from the CDF charts (Appendix F). There are, of course, currently no actual accuracy requirements for non-aviation users and the simulation was performed with the assumption of no satellite failures. These charts show that the combined constellation produces dramatic effects on availability.

3.3.3 Urban Global Study - 15° Mask angle

The urban global study shows the effects on HPE for all the signals and receivers considered in the previous cases for the peak solar period, and all sites in the world considered urban. The 15º mask angle represents minimum elevation at which the multipath model used (Jahn) provides statistical information about the signals.

As it can be observed in Figure 3-6, HPE improvement is very significant, from more than 11m HPE in each single constellation case to about 6.5m in the dual case (SF BOC(1,1)) that is more than 40% accuracy improvement. The advantages of MBOC versus BOC(1,1) using these multipath assumptions are shown in the figures. As explained earlier, partial correlation between satellites of the ionospheric error is assumed for single frequency receivers and not for dual frequency receivers, which affects the DF case performances. However, the DF case is maintained to illustrate the improvement from the combined use. It should be noted that the maximum scale of the color bar of Figure 3-6 was changed from 6m to 12m.

3.3.4 Urban Global Study - 30° Mask Angle

This study is equivalent to the previous Urban Global Study – 15º Mask Angle, but in this study, signals from elevation angles lower than 30º are discarded. This case can be considered as a measure of availability in hard urban environments, where direct lines of sight below 30º very often cannot be seen. The same figures as in the Urban Global Study-15º Mask Angle are provided.

Figure 3-7 shows the same trends as in the 15º case, but the overall accuracy is lower here, e.g. 6.45m (15º) versus 8.02m (30º) for the SF BOC(1,1) dual constellation case.

Table 3-4 shows an average availability of 57.28% and 75.02% for GPS and Galileo respectively, and 98.93% in the dual case. This case again demonstrates a dramatic availability improvement due to the combination of both constellations, showing a remarkable improvement in low visibility areas as well as deep urban ones, where non-aviation users are often located when computing their position fix.

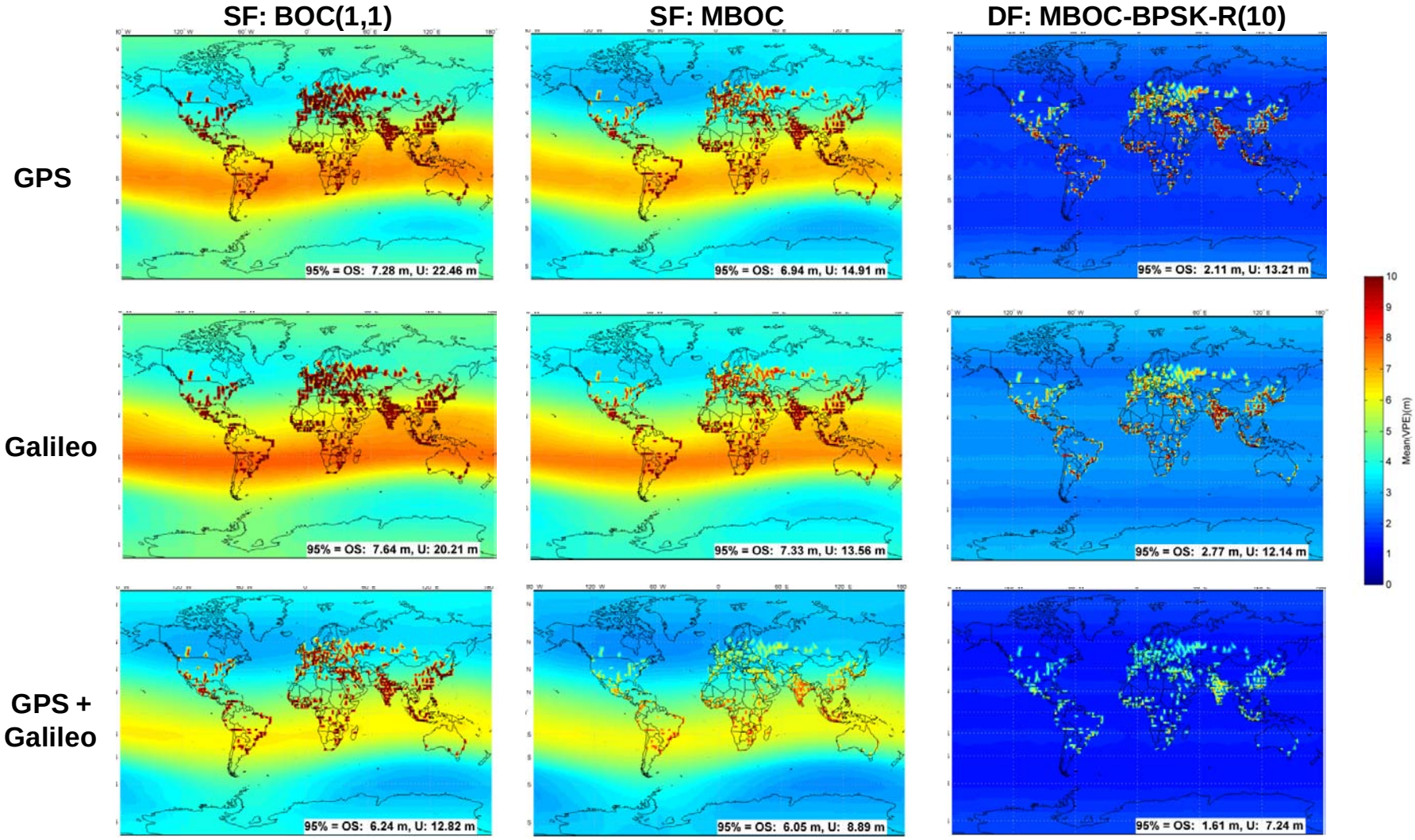

Figure 3-1: Principal Study - Comparison of Mean VPE(m) for Average Solar Cycle

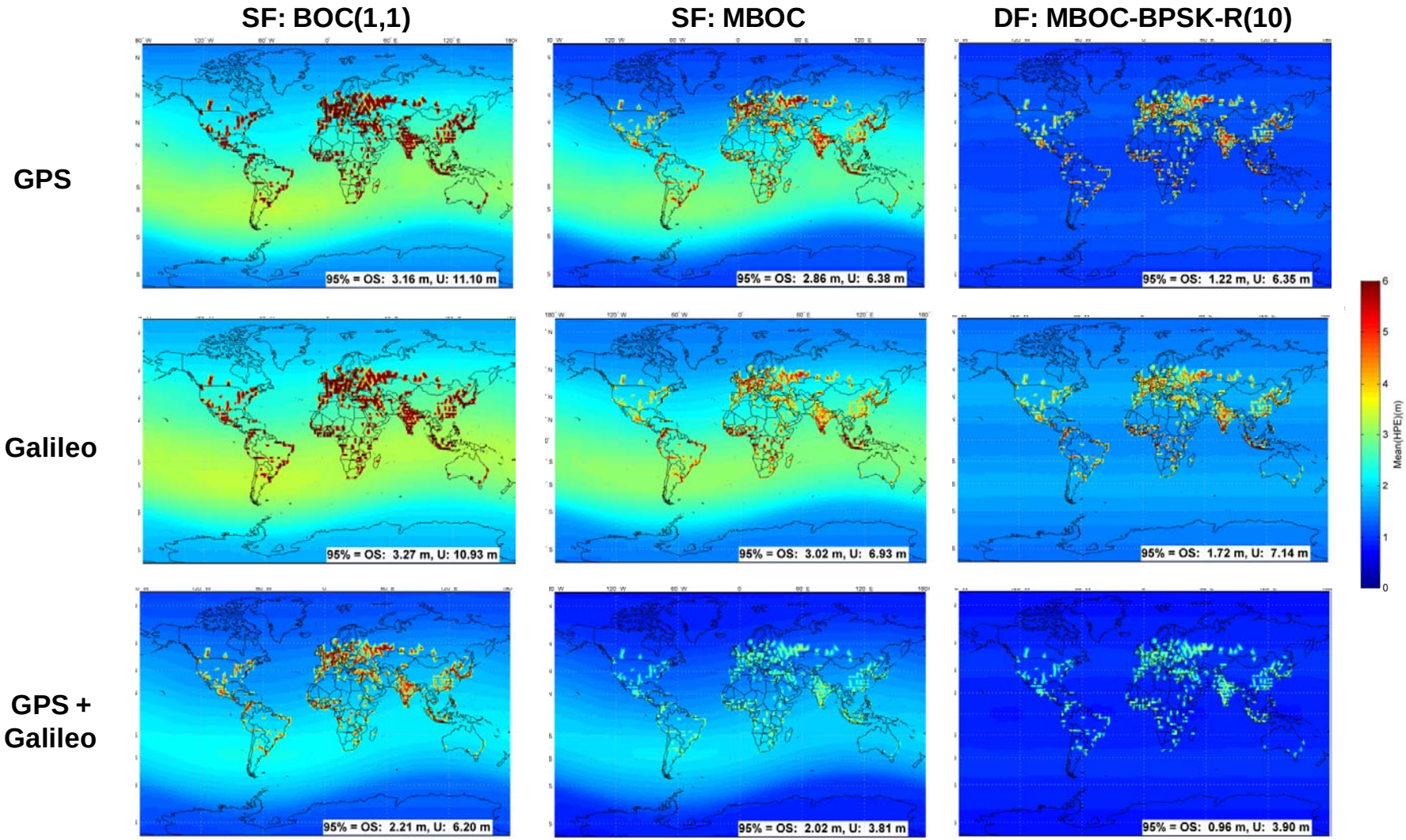

Figure 3-2: Principal Study - Comparison of Mean HPE(m) for Average Solar Cycle

VPE

		SF: BOC(1,1)		SF: MBOC		DF: MBOC-BPSK10	
	VPE	Open Sky	Urban	Open Sky	Urban	Open Sky	Urban
GPS	%ge pdop = 10 & nsat = 4	100%	99.42%	100%	99.42%	100%	99.42%
	mean	5.61	19.74	5.17	12.21	1.76	10.45
	stdev	1.27	1.92	1.36	1.85	0.15	1.83
	RMS	5.76	19.83	5.34	12.35	1.76	10.61
	Median	5.77	19.97	5.35	12.50	1.73	10.38
	95th	7.28	22.46	6.94	14.91	2.11	13.21
Galileo	%ge pdop = 10 & nsat = 4	100%	100%	100%	100%	100%	100%
	mean	5.91	17.58	5.55	11.39	2.58	9.80
	stdev	1.26	1.88	1.31	1.53	0.14	1.59
	RMS	6.05	17.68	5.70	11.49	2.58	9.93
	Median	6.11	17.60	5.74	11.71	2.56	10.11
	95th	7.64	20.21	7.33	13.56	2.77	12.14
GPS & Galileo	%ge pdop = 10 & nsat = 4	100%	100%	100%	100%	100%	100%
	mean	4.76	11.58	4.50	7.38	1.39	6.14
	stdev	1.12	0.92	1.18	1.04	0.10	0.77
	RMS	4.89	11.62	4.66	7.46	1.39	6.19
	Median	4.89	11.81	4.64	7.42	1.37	6.19
	95th	6.24	12.82	6.05	8.89	1.61	7.24

HPE

		SF: BOC(1,1)		SF: MBOC		DF: MBOC-BPSK10	
	HPE	Open Sky	Urban	Open Sky	Urban	Open Sky	Urban
GPS	%ge pdop = 10 & nsat = 4	100%	99.42%	100%	99.42%	100%	99.42%
	mean	2.56	9.81	2.20	5.66	1.13	5.50
	stdev	0.45	0.56	0.52	0.42	0.06	0.48
	RMS	2.60	9.82	2.26	5.68	1.14	5.52
	Median	2.64	9.64	2.31	5.62	1.13	5.43
	95th	3.16	11.10	2.86	6.38	1.22	6.35
Galileo	%ge pdop = 10 & nsat = 4	100%	100%	100%	100%	100%	100%
	mean	2.78	8.74	2.47	5.26	1.62	5.34
	stdev	0.42	1.05	0.46	0.76	0.08	0.76
	RMS	2.81	8.80	2.51	5.31	1.62	5.39
	Median	2.88	8.34	2.57	5.03	1.63	5.01
	95th	3.27	10.93	3.02	6.93	1.72	7.14
GPS & Galileo	%ge pdop = 10 & nsat = 4	100%	100%	100%	100%	100%	100%
	mean	1.84	5.60	1.61	3.19	0.90	3.33
	stdev	0.30	0.33	0.34	0.29	0.04	0.27
	RMS	1.87	5.61	1.64	3.21	0.90	3.34
	Median	1.91	5.50	1.69	3.09	0.90	3.24
	95th	2.21	6.20	2.02	3.81	0.96	3.90

Table 3-1: Principal Study - Global Statistics of Mean VPE and HPE (m) for Average Solar Cycle

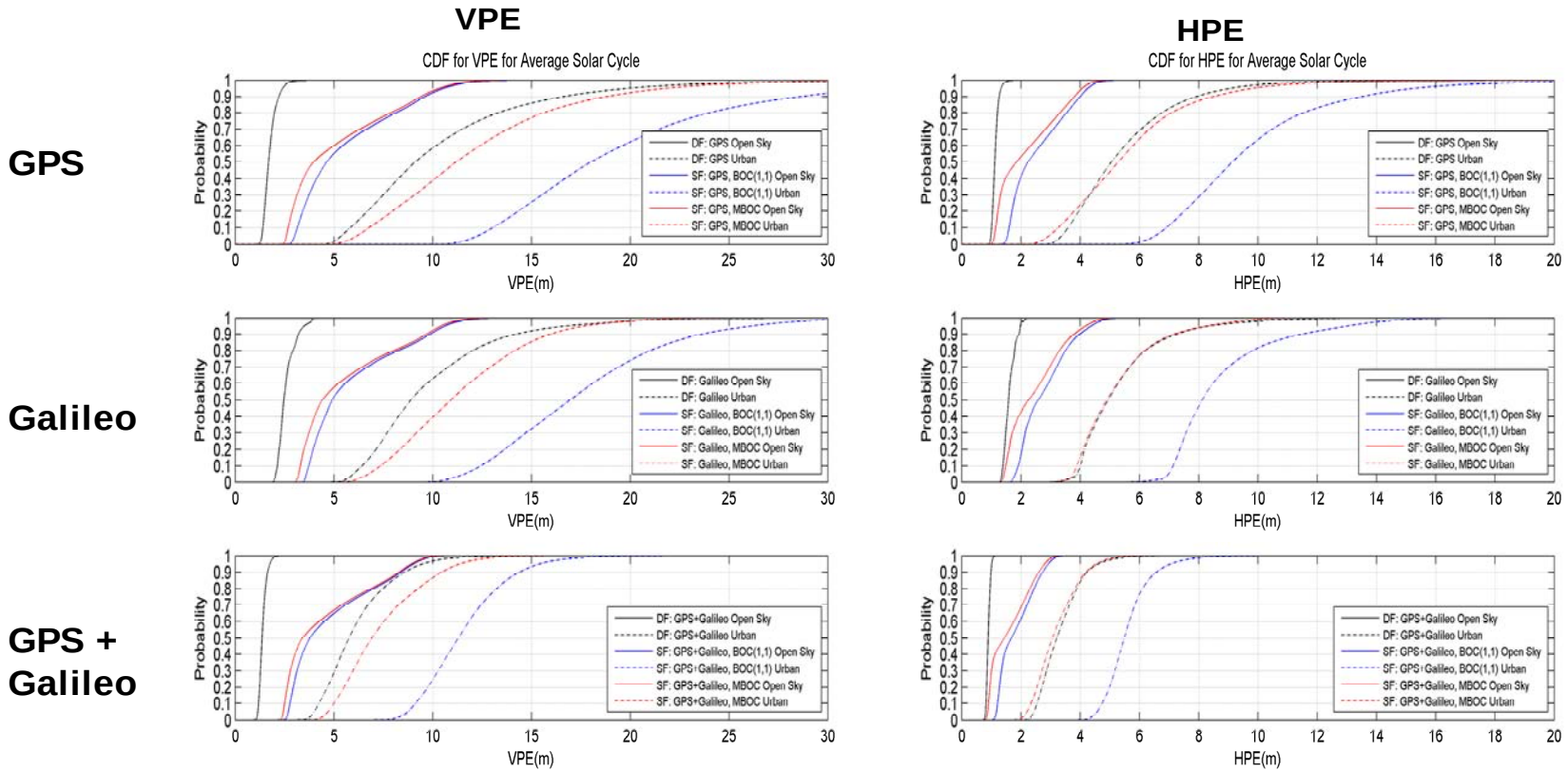

Figure 3-3: Principal Study - Empirical CDFs of All Values of VPE and HPE for Average Solar Cycle

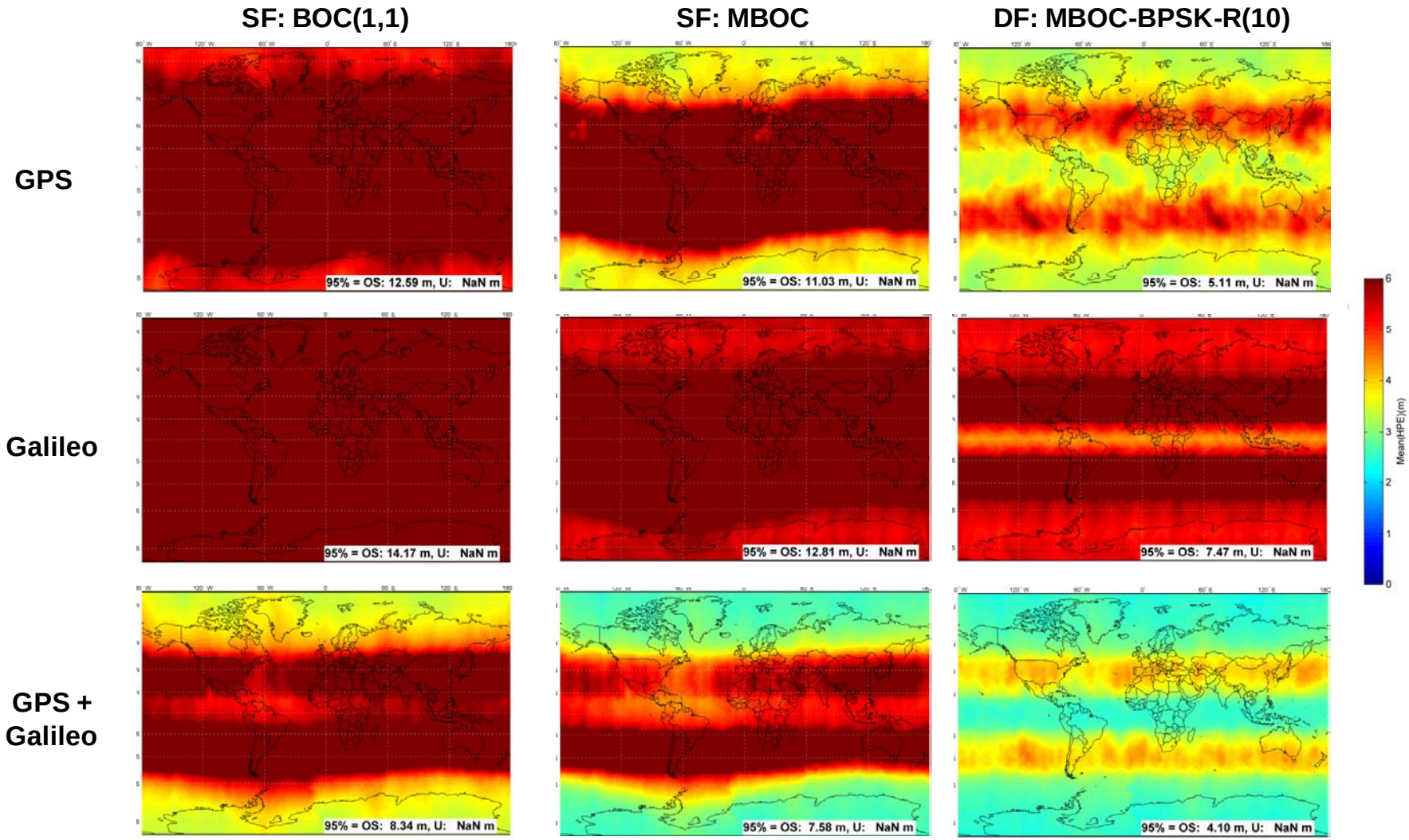

Figure 3-4: Half-Sky Study - Comparison of Half Sky Mean HPE(m) for Average Solar Cycle

VPE

		SF: BOC(1,1)	SF: MBOC	DF: MBOC-BPSK10
	VPE	**Open Sky**	**Open Sky**	**Open Sky**
GPS	**%ge pdop • 10 & nsat • 4**	63.16%	63.16%	63.16%
	mean	10.12	8.61	3.88
	stdev	2.08	2.30	0.34
	RMS	10.33	8.91	3.89
	Median	10.31	8.89	3.82
	95th	13.22	11.98	4.50
Galileo	**%ge pdop • 10 & nsat • 4**	78.57%	78.57%	78.57%
	mean	10.92	9.67	5.60
	stdev	2.93	2.77	1.06
	RMS	11.30	10.06	5.70
	Median	11.05	9.91	5.40
	95th	15.78	14.28	7.30
GPS & Galileo	**%ge pdop • 10 & nsat • 4**	98.92%	98.92%	98.92%
	mean	7.43	6.71	3.09
	stdev	1.63	1.70	0.45
	RMS	7.61	6.92	3.13
	Median	7.66	6.97	3.06
	95th	10.02	9.35	3.79

HPE

		SF: BOC(1,1)	SF: MBOC	DF: MBOC-BPSK10
	HPE	**Open Sky**	**Open Sky**	**Open Sky**
GPS	**%ge pdop • 10 & nsat • 4**	63.16%	63.16%	63.16%
	mean	9.39	7.68	4.08
	stdev	1.94	2.08	0.60
	RMS	9.59	7.96	4.12
	Median	9.33	7.77	3.96
	95th	12.59	11.03	5.11
Galileo	**%ge pdop • 10 & nsat • 4**	78.57%	78.57%	78.57%
	mean	10.48	9.09	6.11
	stdev	2.18	2.17	1.02
	RMS	10.70	9.35	6.20
	Median	10.42	9.01	6.25
	95th	14.17	12.81	7.47
GPS & Galileo	**%ge pdop • 10 & nsat • 4**	98.92%	98.92%	98.92%
	mean	6.11	5.28	3.22
	stdev	1.30	1.36	0.57
	RMS	6.24	5.45	3.27
	Median	6.05	5.31	3.18
	95th	8.34	7.58	4.10

Table 3-2: Half-Sky Study - Global Statistics of Mean VPE and HPE for Average Solar Cycle

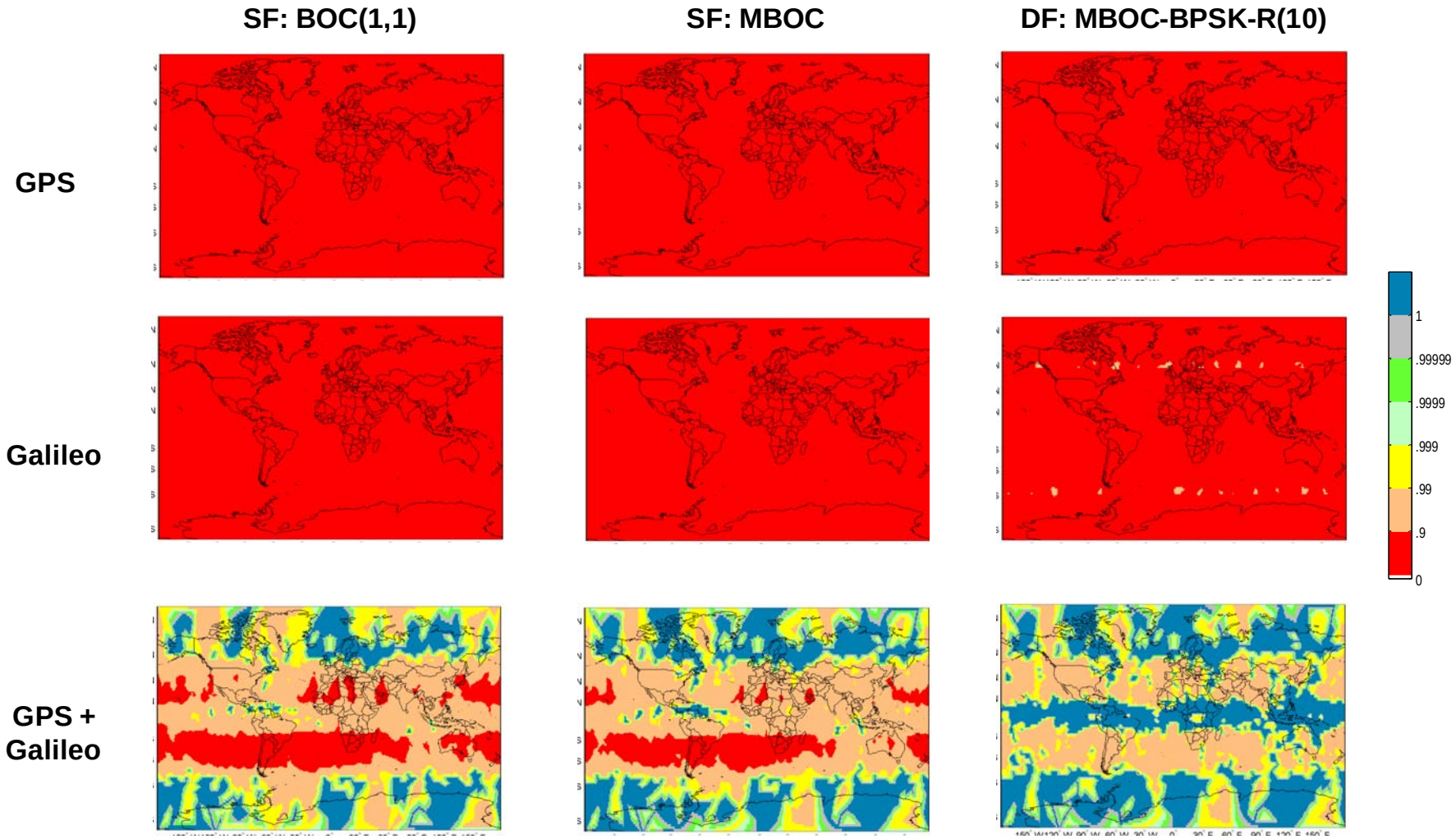

Figure 3-5: Half Sky Study - Availability of Accuracy (H=12m; V=14m); no satellite failure

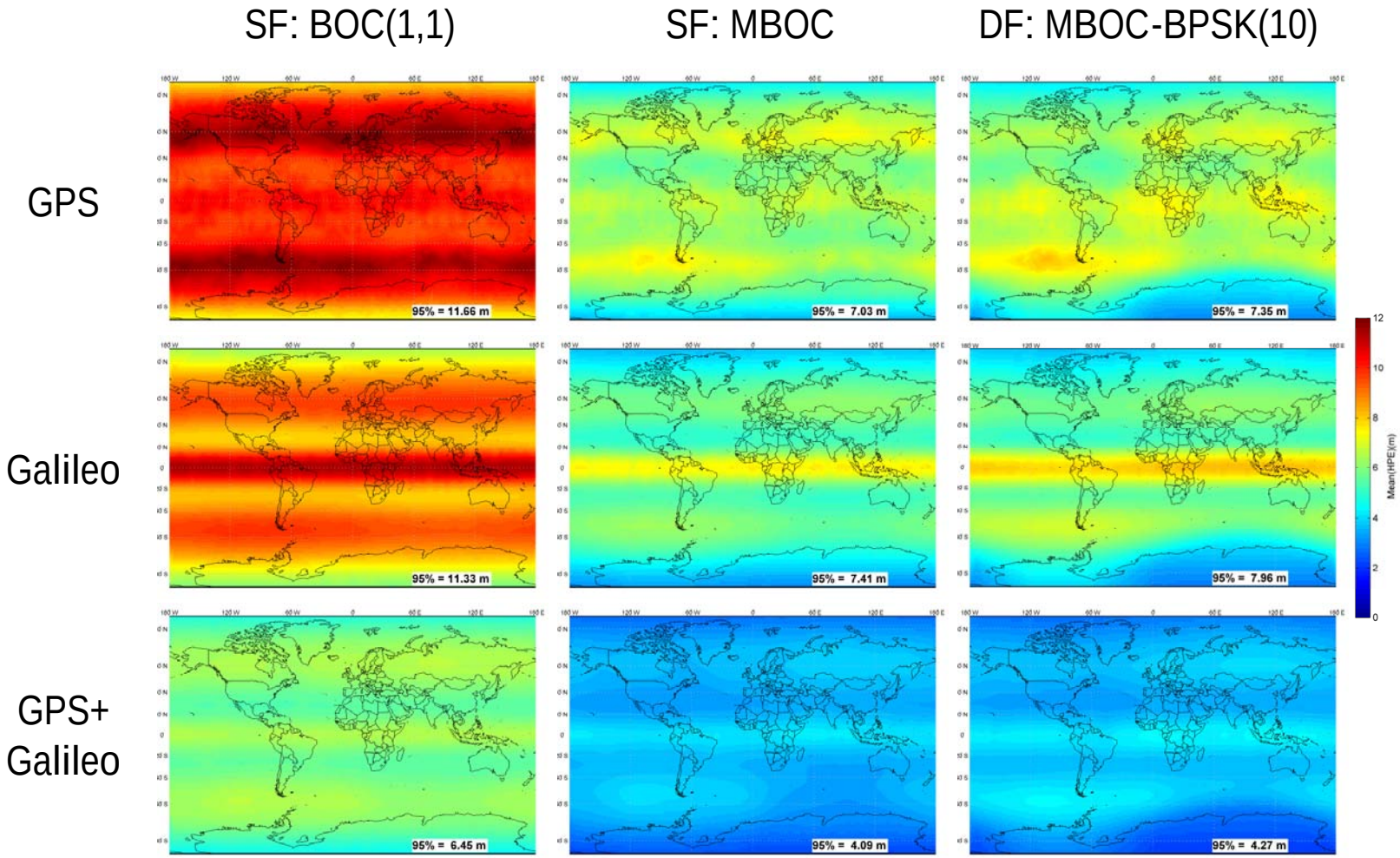

Figure 3-6: Urban Global Study (15º) -Comparison of Mean HPE(m) for Peak Solar Cycle

VPE		BOC(1,1)	MBOC	Dual Frequency
		Urban	Urban	Urban
GPS	Availability [%]	99,10	99,10	99,10
	Mean [m]	21,43	14,12	12,74
	StDev [m]	2,49	1,85	1,90
	RMS [m]	21,57	14,24	12,88
	Median [m]	21,79	14,52	13,03
	95th perc. [m]	24,41	16,29	15,45
Galileo	Availability [%]	100,00	100,00	100,00
	Mean [m]	18,51	12,69	11,30
	StDev [m]	2,16	1,65	1,80
	RMS [m]	18,63	12,80	11,44
	Median [m]	18,56	13,09	11,59
	95th perc. [m]	21,30	14,94	13,86
GPS + Galileo	Availability [%]	100,00	100,00	100,00
	Mean [m]	12,81	8,89	7,17
	StDev [m]	1,33	1,16	0,84
	RMS [m]	12,88	8,96	7,22
	Median [m]	13,16	9,22	7,42
	95th perc. [m]	13,91	10,11	8,04

HPE		BOC(1,1)	MBOC	Dual Frequency
		Urban	Urban	Urban
GPS	Availability [%]	99,10	99,10	99,10
	Mean [m]	10,24	6,26	6,43
	StDev [m]	0,73	0,49	0,68
	RMS [m]	10,26	6,28	6,46
	Median [m]	10,09	6,27	6,50
	95th perc. [m]	11,66	7,03	7,35
Galileo	Availability [%]	100,00	100,00	100,00
	Mean [m]	9,20	5,81	6,11
	StDev [m]	1,11	0,82	1,03
	RMS [m]	9,27	5,87	6,19
	Median [m]	9,08	5,65	5,89
	95th perc. [m]	11,33	7,41	7,96
GPS + Galileo	Availability [%]	100,00	100,00	100,00
	Mean [m]	5,94	3,62	3,74
	StDev [m]	0,36	0,29	0,36
	RMS [m]	5,95	3,64	3,76
	Median [m]	5,93	3,62	3,73
	95th perc. [m]	6,45	4,09	4,27

Table 3-3: Urban Global Study (15º) – Global Statistics of Mean HPE and VPE for Peak Solar Cycle

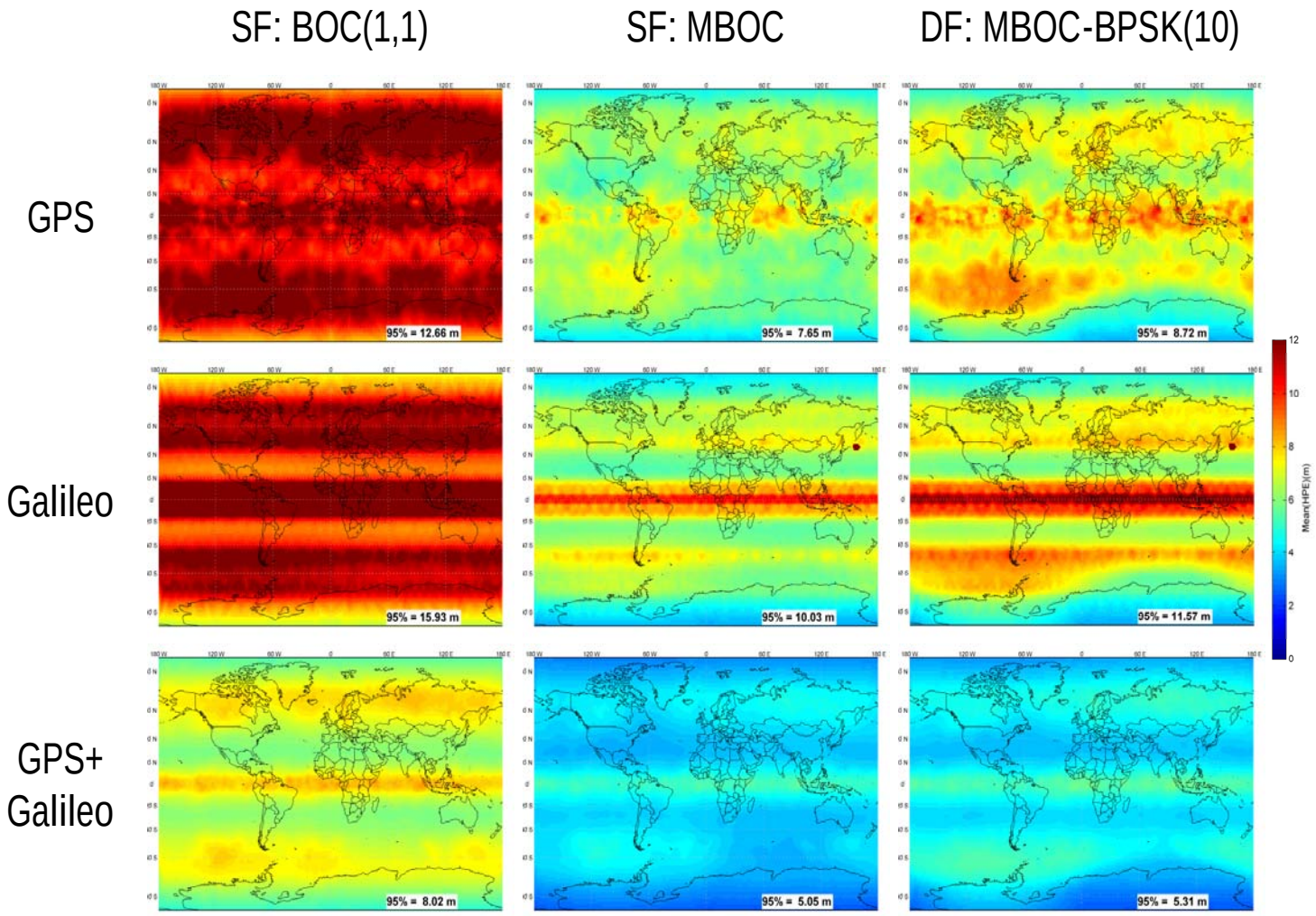

Figure 3-7: Urban Global Study (30º) -Comparison of Mean HPE(m) for Peak Solar Cycle

VPE		BOC(1,1)	MBOC	Dual Frequency
		Urban	Urban	Urban
GPS	Availability [%]	57,28	57,28	57,28
	Mean [m]	25,68	15,25	16,13
	StDev [m]	4,11	2,74	2,98
	RMS [m]	26,01	15,50	16,41
	Median [m]	24,66	14,87	15,61
	95th perc. [m]	32,21	19,97	21,26
Galileo	Availability [%]	75,02	75,02	75,02
	Mean [m]	24,35	15,53	16,00
	StDev [m]	4,14	2,81	3,08
	RMS [m]	24,70	15,79	16,30
	Median [m]	24,02	15,60	16,01
	95th perc. [m]	29,85	19,46	20,39
GPS + Galileo	Availability [%]	98,93	98,93	98,93
	Mean [m]	16,57	10,64	10,07
	StDev [m]	2,38	1,67	1,52
	RMS [m]	16,74	10,77	10,19
	Median [m]	16,60	10,84	10,10
	95th perc. [m]	19,44	12,88	12,07

HPE		BOC(1,1)	MBOC	Dual Frequency
		Urban	Urban	Urban
GPS	Availability [%]	57,28	57,28	57,28
	Mean [m]	11,19	6,43	7,26
	StDev [m]	0,93	0,69	0,90
	RMS [m]	11,23	6,47	7,32
	Median [m]	11,14	6,40	7,24
	95th perc. [m]	12,66	7,65	8,72
Galileo	Availability [%]	75,02	75,02	75,02
	Mean [m]	11,36	6,97	7,85
	StDev [m]	2,16	1,52	1,86
	RMS [m]	11,56	7,13	8,07
	Median [m]	11,31	6,68	7,52
	95th perc. [m]	15,93	10,03	11,57
GPS + Galileo	Availability [%]	98,93	98,93	98,93
	Mean [m]	6,82	4,11	4,37
	StDev [m]	0,70	0,49	0,54
	RMS [m]	6,86	4,14	4,40
	Median [m]	6,71	4,03	4,30
	95th perc. [m]	8,02	5,05	5,31

Table 3-4: Urban Global Study (30º) – Global Statistics of Mean VPE and HPE for Peak Solar Cycle

4 CONCLUSIONS

This note presents the user performances for future GPS-III, Galileo and combined GPS-III/Galileo in different study cases, including open, urban and half occluded environments, as well as different ionospheric activity periods. All study cases were analysed for three different receivers of increasing performance and complexity.

The studies demonstrate and quantify the improvements that can be expected when using GPS and Galileo open services in combination under different environmental conditions. In all studied cases, the combination of GPS and Galileo led to noteworthy performance improvements as compared to single system performance. The most significant improvement is for partially obscured environments, where buildings, trees or terrain block portions of the sky. The increased number of satellites available provides robust performance even as some signals are blocked, which is reflected in a significant increase of positioning accuracy and availability.

The results also confirm that dual-frequency receivers provide an improvement over single-frequency in most environments, and the best performances were generally achieved with a dual-frequency dual-constellation receiver.

The document also highlights the benefit expected from future broadband signals on GPS L1 and Galileo E1 signals designed in accordance with the joint EU-US agreement reached in 2006.

This work concludes the first stage of activities in the context of the EU-US Working Group C on the next generation of civil satellite-based navigation and timing systems. It confirms that the two systems, thanks to their interoperable and compatible signal baselines, can easily be integrated and processed by civil user equipment and that such a combined use offers tremendous benefits to a broad range of user communities.

It is intended that further synergies will be investigated in the context of Working Group C for the future generations of GPS and Galileo systems, with the objective to offer ever-improving combined service performance to civil users through US and EU cooperation. Future activities of the Working Group will address other services and an even broader range of civil user communities. These studies are intended to serve as a precedent for future analyses on combined performance of different systems and services and to facilitate multilateral discussions in other forums.

EU-US Cooperation on Satellite Navigation - Working Group C

Combined Performances for Open GPS/Galileo Receivers

APPENDIXES

Appendix A ..... - 1 -
Appendix B ..... - 13 -
Appendix C ..... - 15 -
Appendix D ..... - 19 -
Appendix E ..... - 25 -
Appendix F ..... - 27 -
Appendix G ..... - 44 -

Appendix A

Multipath Models for BPSK-R(10), BOC(1,1), and MBOC for Urban, Suburban, and Open Sky Environments

A.1 Approach

The approach for developing multipath models is as follows:

1. Use Jahn's method [6] to generate the amplitudes, phases and delays of the direct and multipath signals for urban, suburban, and open sky environments,
2. Compare Jahn's open sky results with those used previously such as the Mats Brenner method,
3. Using the discriminator function (S-curve) for a non-coherent discriminator (e.g., dot-product), determine the zero crossings with and without multipath [9], and
4. Multipath error (meters) = difference of zero crossings with and without multipath in chips x chip width in meters.

A.2 Dot-Product Discriminator Function [7-9]

The dot-product non-coherent discriminator function without multipath is given by [7-9]:

$$D(\mathrm{t}) = a_0[R(\mathrm{t} - d/2) - R(\mathrm{t} + d/2)]R(\mathrm{t}) \qquad \text{(A-1)}$$

and with multipath is given by:

$$D(\tau) = a_0\left[\left(R(\tau - d/2) - R(\tau + d/2)\right)\cos\left(\phi + \sum_{i=1}^{M} a_i\left(R(\tau - d/2 - \delta_i) - R(\tau + d/2 - \delta_i)\right)\cos\left(\phi + \phi_i\right)\right)\right] \times$$
$$\left(R(\tau)\cos\left(\phi + \sum_{i=1}^{M} a_i R(\tau - \delta_i)\cos\left(\phi + \phi_i\right)\right)\right)$$
$$+ a_0\left[\left(R(\tau - d/2) - R(\tau + d/2)\right)\sin\left(\phi + \sum_{i=1}^{M} a_i\left(R(\tau - d/2 - \delta_i) - R(\tau + d/2 - \delta_i)\right)\sin\left(\phi + \phi_i\right)\right)\right] \times$$
$$\left(R(\tau)\sin\left(\phi + \sum_{i=1}^{M} a_i R(\tau - \delta_i)\sin\left(\phi + \phi_i\right)\right)\right) \qquad \text{(A-2)}$$

where:

$R(\tau) = \text{autocorrelation function}$

$a_i = \dfrac{a_i}{a_0}, \tilde{\phi} + \phi_i = \theta_i - \theta_0, \tilde{\phi} = -\theta_0$

$a_0 = (1 - A)a_{0,LOS} + Aa_{0,Shadow} = \text{amplitude of direct signal}$

$A = \text{probability of shadow given by Jahn [6]}$

$M = N_n + N_f$

$N_n = \text{number of near echoes}$

$N_f = \text{number of far echoes}$

$\delta = \text{spacing between early and late gate (0.1 is assumed)}$

A.3 Autocorrelation Functions (ACFs)

The autocorrelation functions (ACFs) of the BOC(1,1), MBOC, and BPSK-R(10) signals are shown in Figure A-1. These ACFs are filtered by a 2-sided bandwidth equal to 4MHz for BOC(1,1), 14MHz for MBOC, and 20MHz for BPSK-R(10) filters.

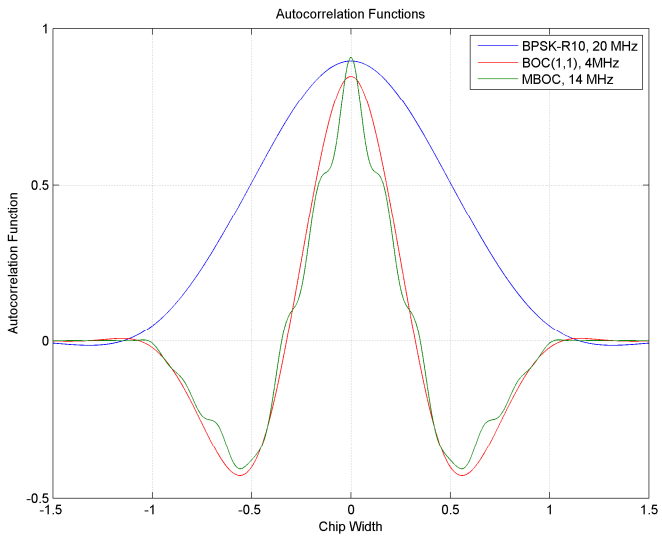

Figure A-1. Autocorrelation Functions

A.4 Dot-Product Non-coherent Discriminator Function (S-Curve)

The Dot-Product Non-coherent Discriminator Functions (S-Curve) of the three signals without multipath are shown in Figure A-2. These are calculated using Equation (A-1) and the ACFs shown in Figure A-1.

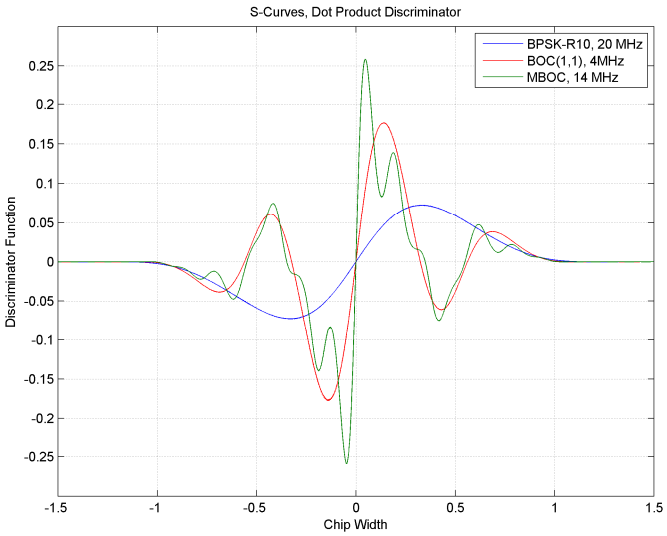

Figure A-2. Dot-Product Non-coherent Discriminator Function (S-Curve) without Multipath

A.5 Summary of Jahn Multipath Method

Jahn et al. [6] explains in detail the characteristics of satellite propagation channels for spread spectrum communications. This reference presented a wideband channel model for land mobile satellite (LMS) services which characterizes the time-varying transmission channel between a satellite and a mobile user terminal. It is based on a measurement campaign at L-band. The parameters of the model are the results of fitting procedures to measured data. The parameters are tabulated in Jahn et al. [6] for various environments and elevation angles. The focus in this section is on the implementation of Jahn's method in the urban, suburban and open sky environments for a ground user and many passages come directly from his paper.

The complex impulse response of the satellite wideband channel can be superimposed to a sum of k = 1, 2, … , N signal paths with complex amplitude $E_k(t)$ and delay $\tau_1(t)$ and $\tau_k(t)=\tau_1(t)+\Delta\tau_k(t)$, k=2, 3, …, N:

$$h(\tau,t)=\sum_{k=1}^{N}E_k(t)\delta(\tau-\tau_k(t)) \qquad \text{(A-3)}$$

The amplitude of each echo is complex as follows:

$$E_k(t)=a_k(t)e^{j\phi_k(t)} \qquad \text{(A-4)}$$

For a wide-sense stationary with uncorrelated scatterers (WSSUS) channel, the phases $\phi_k(t)$ are uniformly distributed random variables in the range $[0,2\pi]$.

The channel impulse response with N echoes can be divided into three parts with different behavior. These parts are: direct path, near echoes, and far echoes and are described as follows [6]:

1. **The direct path a_0:**

The direct path is modeled as follows:

$a_0 = (1-A)a_{0,LOS} + Aa_{0,Shadow}$ = amplitude of direct signal, where:

A = probability of shadow given in Table A-1.

It should be noted that $a_{0,LOS}$ and $a_{0,Shadow}$ are generated using Rician and Rayleigh random number generators, respectively. In the LOS environment, the probability density function (pdf) of the Rice distribution is given as follows:

$$f_{Rice}(a_{0,LOS}) = \frac{a_{0,LOS}}{\sigma^2} I_0\left(\frac{a_{0,LOS}}{\sigma^2}\right)\exp\left(-\frac{a_{0,LOS}^2+1}{2\sigma^2}\right) \quad \text{(A-5)}$$

with a Rice-factor $c = \frac{1}{2\sigma^2}$ denoting the carrier-to-multipath ratio.

In the shadow environments, the pdf of the Rayleigh distribution is given by:

$$f_{Rayleigh}(a_{0,Shadow}) = \frac{a_{0,Shadow}}{\sigma^2}\exp\left(-\frac{a_{0,Shadow}^2}{2\sigma^2}\right) \quad \text{(A-6)}$$

with a mean power ($P_0 = 2\sigma^2$) distributed as log-normal as follows:

$$f_{\log-normal}(P_0) = \frac{10}{\sigma\sqrt{2\pi}\ln(10)P_0}\exp\left(-\frac{(10\log P_0 - \mu)^2}{2\sigma^2}\right) \quad \text{(A-7)}$$

The parameters of these distributions are shown in Table A-1 for different environments and elevation angles.

Table A-1. Model Parameters for the Direct Path

	Shadowing probability	a_0,LOS (Rice factor)	a_0,Shadow, (Rayleigh)	
Parameter	**A**	**c(dB)**	**m(dB)**	**s(dB)**
Environment				
Open Sky				
E (deg)				
15	0.00	6.0	---	---
25	0.00	10.3	---	---
35	0.00	12.0	---	---
45	0.00	10.4	---	---
55	0.00	9.0	---	---
Suburban				
E (deg)				
15	0.77	4.7(1)	-12.6	4.8
25	0.59	4.7	-6.0	3.5
35	0.54	10.7	-7.6	3.2
45	0.43	4.0	-7.2	3.2
55	0.35	11.8	-7.7	2.6
Urban				
E (deg)				
15	0.97	9.0(1)	-15.2	5.2
25	0.79	3.2	-12.1	6.3
35	0.60	4.8	-4.4	5.1
45	0.56	8.5	-3.0	2.7
55	0.30	6.0	-3.0(1)	2.7(1)

Notes: (1) Missing data are estimated

2. **The region of near echoes**:

A number (N_n) of near echoes appear in the close vicinity of the receiver with delays $0 < \Delta t_k^n \le t_e = 600ns$. Most of the echoes will appear in this delay interval. The number of near echoes, N_n, follows a Poisson distribution as follows:

$$f_{Poisson}(N) = \frac{\lambda^N}{N!} e^{-\lambda} \tag{A-8}$$

where the values of the parameter (λ) are given in Table A-2 for different environments and different elevation angles.

The mean power of the near echoes is:

$$S(t) = S_0 e^{-dt} \; S(t) = S_0 e^{-dt} \tag{A-9}$$

or in log scaling,

$$S(t)(dB) = S_0(dB) - d(dB)t \; S(t)(dB) = S_0(dB) - d(dB)t \tag{A-10}$$

Where

$$d(dB) = \frac{10\log_{10}(d)}{10\log_{10}(e)} \; d(dB) = \frac{10\log_{10}(d)}{10\log_{10}(e)} \tag{A-11}$$

Given a mean echo power S(τ) for a fixed delay τ, the amplitude $a_k^{(n)}$ of the near echoes will vary around this mean value according to a Rayleigh distribution with $2\sigma^2 = S(t)$ according to Equation A-6.

The near echoes delay Δt_k^n distribution follows an exponential distribution as follows:

$$f_{\exp}(\Delta t_k) = \frac{1}{b} e^{-\frac{\Delta t_k}{b}} \; f_{\exp}(\Delta t_k) = \frac{1}{b} e^{-\frac{\Delta t_k}{b}} \tag{A-12}$$

Table A-2 shows the parameters for the near echoes.

Table A-2. Model Parameters for Near Echoes

	N(n), Poisson	max delay	Delay $Dt^{(n)}$ exp	S(t)	
Parameter	l	t_e(ns)	**b (ms)**	**S0(dB)**	**d(dB)**
Environment					
Open Sky					
E (deg)					
15	1.6	400	0.033	-28.5	3.0
25	1.2	400	0.030	-28.6	1.0
35	1.2	400	0.027	-25.7	9.5
45	0.5	400	0.027	-29.0	1.1
55	0.5(1)	400	0.027(1)	-29.0(1)	1.1(1)
Suburban					
E (deg)					
15	1.2	400	0.037	-22.6	-21.9
25	1.4	400	0.038	-23.8	23.7
35	1.2	400	0.039	-24.9	19.4
45	1.5	400	0.027	-24.4	23.0
55	1.6	400	0.033	-24.7	18.7
Urban					
E (deg)					
15	1.2	600	0.118	-16.5	11.0
25	4.0	600	0.063	-17.0	26.2
35	3.5	600	0.069	-23.6	6.5
45	3.6	600	0.081	-23.5	8.5
55	3.8	600	0.079	-26.1	6.3

Notes: (1) Missing data are estimated

3. **The region of far echoes**:

A number (N_f = N-N_n-*1*) of the far echoes follows a Poisson distribution as shown in Equation (A-8). The far echoes appear with delays $t_e < \Delta t_k^f \le t_{max}$. Only a few echoes with long delays could be observed. These delays are uniformly distributed in the range $[t_e, t_{max})$. The amplitudes $a_k^{(f)}$ of the far echoes follow a Rayleigh distribution according to Equation A-6. Table A-3 shows the parameters for the far echoes.

Table A-3. Model Parameters for Far Echoes

	$N^{(f)}$, Poisson	$a_k^{(f)}$ Rayleigh	max delay
Parameter	l	$2s^2$ (dB)	t_{max}(ms)
Environment			
Open Sky			
E (deg)			
15	0.3	-26.4	15
25	0.3(1)	-26.4(1)	15(1)
35	0.3(1)	-26.4(1)	15(1)
45	0.3(1)	-26.4(1)	15(1)
55	0.3(1)	-26.4(1)	15(1)
Mountains			
E (deg)			
15	0.9	-29.0	15
25	1.8	-28.5	15
35	4.4	-23.5	15
45	4.0	-21.7	15
55	4.0(1)	-21.7(1)	15

Notes: (1) Missing data are estimated

A.6 Summary of Results using Jahn's Multipath Method

Figure A-3 shows the urban multipath curves generated by Jahn's method for BOC(1,1), MBOC, and BPSK-R(10) signals. The squares in this figure are the data generated by Jahn's method using 2000 runs for each signal. The solid curves are fitted functions to the data using the following formula:

$$\sigma(meters) = \max\{a + b \cdot \text{atan}(c(E(\text{deg}) - d)), \varepsilon\}, \ \varepsilon = 1 \times 10^{-4} \quad \text{(A-13)}$$

The four coefficients (a, b, c and d) are shown in Table A-4.

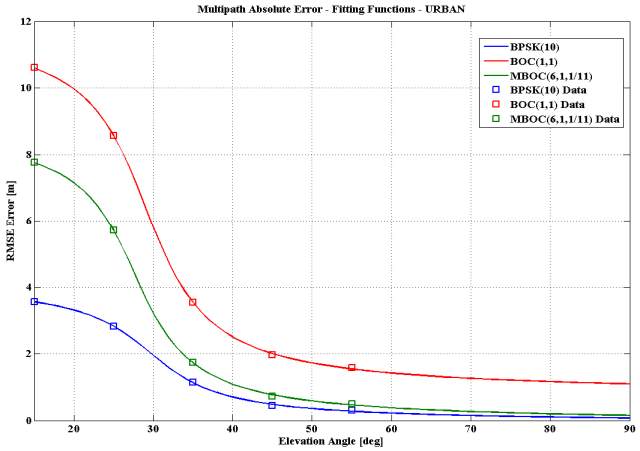

Figure A-3. Urban Multipath Models Generated by Jahn's Method

Figures A-4 and A-5 show the curves for suburban and open sky environments using Jahn's method. The solid curves are fitted functions to the data using the following exponential formula:

$$\sigma(meters) = \max\{a + b \cdot \exp(cE(\text{deg})), \varepsilon\}, \ \varepsilon = 1 \times 10^{-4} \quad \text{(A-14)}$$

The three coefficients (a, b and c) are also included in Table A-4.

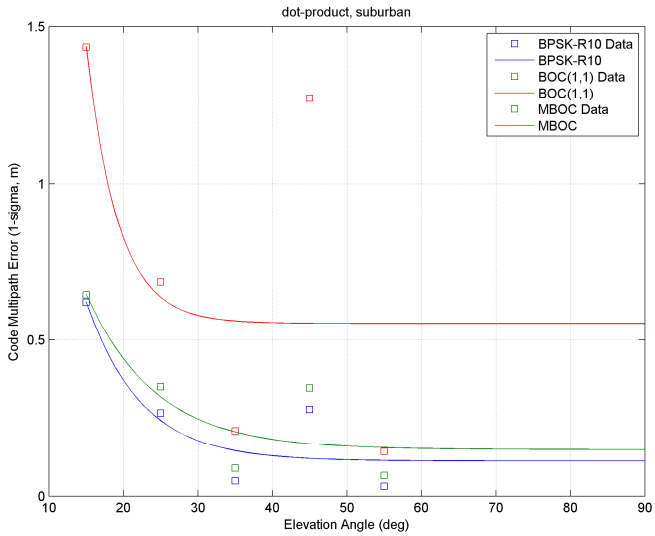

Figure A-4. Suburban Multipath Models Generated by Jahn's Method

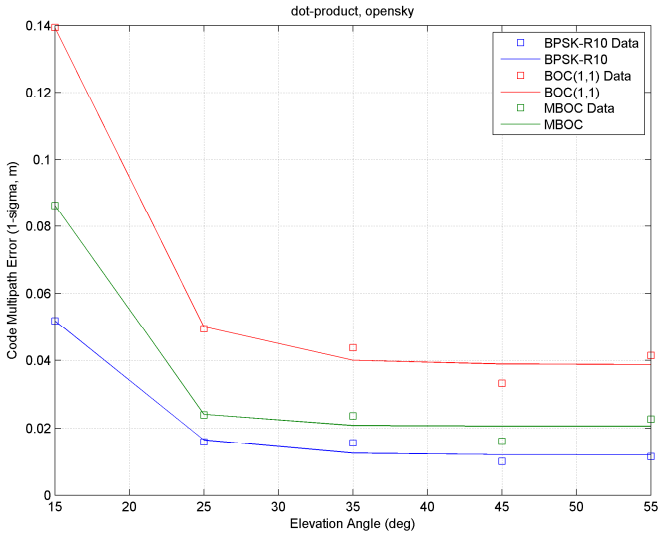

Figure A-5. Open Sky Multipath Models Generated by Jahn's Method

Table A-4. Model Coefficients using Jahn's Method – Urban (fitting with arc-tangent function)

	BOC(1,1)	*MBOC*	*BPSK(10)*
a	6.3784	4.4144	2.0338
b	-3.5782	-2.871	-1.3428
c	0.1725	0.1846	0.1462
d	29.075	27.6112	29.565

Table A-5. Model Coefficients using Jahn's Method – Suburban (fitting with exponential function)

	BOC(1,1)	*MBOC*	*BPSK(10)*
a	0.55349	0.14895	0.11211
b	30.254	2.5236	3.9561
c	-0.23566	-0.10811	-0.13643

Table A-6. Model Coefficients using Jahn's Method – Open Sky (fitting with exponential function)

	BOC(1,1)	*MBOC*	*BPSK(10)*
a	0.038818	0.020649	0.012014
b	2.7128	5.397	1.041
c	-0.21969	-0.29399	-0.2177

A.7 Open Sky Multipath Models using Mats Brenner's Method

References [2 and 3] used Mats Brenner Method to generate multipath models for the GNSS signals including BOC(1,1), MBOC, and BPSK-R(10) for the open sky environment. The details of this method are included in Reference [12] and summarized in Reference [2]. In this model, 500 small reflectors are randomly located within 100 m of the user. Because the reflectors are small, each emanates a spherical wave and thus the received power from each reflector varies with the square of the distance between the reflector and the user. This model was found to closely emulate measured multipath for an aviation differential GPS (DGPS) reference station application with the receiver located in an open environment.

This model has been implemented previously [2, 3] and the results are shown in Figure A-6. The fitted model coefficients using the exponential model shown in Equation A-14 are shown in Table A-5.

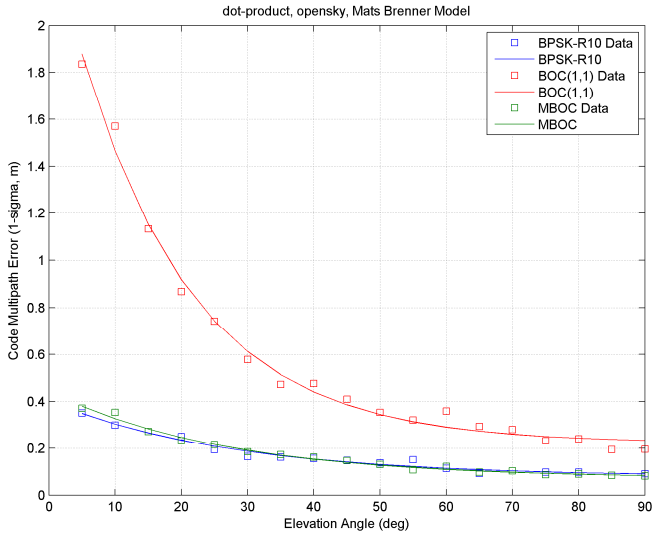

Figure A-6. Open Sky Multipath Models Generated by Mats Brenner's Method

Table A-7. Multipath Model Coefficients using Mats Brenner's Method (fitting with exponential function)

	BOC(1,1)	*MBOC*	*BPSK(10)*
a	0.22176	0.070391	0.077988
b	2.2128	0.37408	0.32624
c	-0.057807	-0.037694	-0.036692

A.8 Comments on the Multipath Modeling Results

- Comparing the Open sky results shown in Figures A-5 and A-6, the multipath error models using Mats Brenner's method are larger than the models using Jahn's Method. Since the models generated by Mats Brenner's method have been validated against actual multipath measurements in open sky, the models shown in Figure A-6 and Table A-5 will be used in the accuracy analysis for open sky.
- Comparing the suburban multipath models shown in Figure A-4 using Jahn's method and the open sky models generated by Mats Brenner's method, it can be seen that the models for both environments (suburban and open sky) are close to each other. Therefore, the suburban environment will not be used in the accuracy analysis.
- For an urban environment, MITRE and University FAF Munich used Jahn's method to generate the urban multipath models.

A.9 Multipath Models to be Used in the Accuracy Analysis

- For urban environments: Jahn's models generated by University FAF Munich (Figure 2-2)
- For open sky environments: Mats Brenner models generated by MITRE (Figure A-6)

Appendix B

Combined GPS/Galileo Constellation

B.1 Almanacs for GPS and Galileo

GPS almanacs for 24-slot constellation are defined in Table A.2-1, GPS-SPS, 4th Edition, September 2008. The Right Ascension of Ascending Node (RAAN) = $OMEGA_0$ + GMST (at July, 1, 1993,0,0,0). This is shown in Table B-1. Galileo almanacs for 27 satellites, 3 planes are shown in Table B-2. Both constellations are synchronized for the July 1, 1993 (hh:mm:ss = 00:00:00) epoch which is equivalent to June 15, 2009, (hh:mm:ss = 01:02:25.1). The Greenwich Mean Sidereal Time (GMST) is identical for both of these epochs (= 279.0555 degrees).

Table B-1. Almanacs for 24 GPS Satellites (6 planes)

PRN No.	Semimajor Axis (m)	Eccentricity (deg)	Inclination (deg)	RAAN (deg)	Angle of Perigee	Mean Anomaly (deg)
1	26559710	0	55	276.79	0	268.126
2	26559710	0	55	276.79	0	161.786
3	26559710	0	55	276.79	0	11.676
4	26559710	0	55	276.79	0	41.806
5	26559710	0	55	336.79	0	80.956
6	26559710	0	55	336.79	0	173.336
7	26559710	0	55	336.79	0	309.976
8	26559710	0	55	336.79	0	204.376
9	26559710	0	55	36.79	0	111.876
10	26559710	0	55	36.79	0	11.796
11	26559710	0	55	36.79	0	339.666
12	26559710	0	55	36.79	0	241.556
13	26559710	0	55	96.79	0	135.226
14	26559710	0	55	96.79	0	265.446
15	26559710	0	55	96.79	0	35.156
16	26559710	0	55	96.79	0	167.356
17	26559710	0	55	156.79	0	197.046
18	26559710	0	55	156.79	0	302.596
19	26559710	0	55	156.79	0	66.066
20	26559710	0	55	156.79	0	333.686
21	26559710	0	55	216.79	0	238.886
22	26559710	0	55	216.79	0	345.226
23	26559710	0	55	216.79	0	105.206
24	26559710	0	55	216.79	0	135.346

Table B-2. Almanacs for 27 Galileo satellites (3 planes)

PRN No.[1]	Semimajor Axis (m)	Eccentricity (deg)	Inclination (deg)	RAAN (deg)	Angle of Perigee	Mean Anomaly (deg)
101	29600000	0	56	30	0.00001	0
102	29600000	0	56	30	0.00001	40
103	29600000	0	56	30	0.00001	80
104	29600000	0	56	30	0.00001	120
105	29600000	0	56	30	0.00001	160
106	29600000	0	56	30	0.00001	200
107	29600000	0	56	30	0.00001	240
108	29600000	0	56	30	0.00001	280
109	29600000	0	56	30	0.00001	320
110	29600000	0	56	150	0.00001	13.33
111	29600000	0	56	150	0.00001	53.33
112	29600000	0	56	150	0.00001	93.33
113	29600000	0	56	150	0.00001	133.33
114	29600000	0	56	150	0.00001	173.33
115	29600000	0	56	150	0.00001	213.33
116	29600000	0	56	150	0.00001	253.33
117	29600000	0	56	150	0.00001	293.33
118	29600000	0	56	150	0.00001	333.33
119	29600000	0	56	270	0.00001	26.66
120	29600000	0	56	270	0.00001	66.66
121	29600000	0	56	270	0.00001	106.66
122	29600000	0	56	270	0.00001	146.66
123	29600000	0	56	270	0.00001	186.66
124	29600000	0	56	270	0.00001	226.66
125	29600000	0	56	270	0.00001	266.66
126	29600000	0	56	270	0.00001	306.66
127	29600000	0	56	270	0.00001	346.66

[1] These PRN numbers correspond only to the satellite identifiers used in the simulations.

Appendix C

VPE and HPE Equations

The Vertical Position Error (VPE) and Horizontal Position Error (HPE) are calculated using the following equations:

$$\begin{aligned} VPE &= 2d_V = 2\sqrt{C(3,3)} \\ HPE &= 2d_{rms} = 2\sqrt{C(1,1)+C(2,2)} \end{aligned} \tag{C-1}$$

where

$$d_{rms} = \sqrt{d_{major}^2 + d_{\text{minor}}^2} = \sqrt{d_{east}^2 + d_{north}^2}$$

Also, $d_{major}, d_{\text{minor}}$ and d_V are defined as follows [1]:

$$\begin{aligned} d_{major} &= \sqrt{\frac{d_{east}^2 + d_{north}^2}{2} + \sqrt{\left(\frac{d_{east}^2 - d_{north}^2}{2}\right)^2 + d_{EN}^2}} \\ d_{\text{minor}} &= \sqrt{\frac{d_{east}^2 + d_{north}^2}{2} - \sqrt{\left(\frac{d_{east}^2 - d_{north}^2}{2}\right)^2 + d_{EN}^2}} \end{aligned} \tag{C-2}$$

$$\begin{aligned} d_{east}^2 &= C(1,1), \quad d_{EN} = C(1,2) \\ d_{north}^2 &= C(2,2), \; d_V^2 = C(3,3) \end{aligned} \tag{C-3}$$

n = number of visible satellites,

$$\text{Covariance Matrix} = C = \left(\mathrm{G}^T \mathrm{W} \mathrm{G}\right)^{-1} = \begin{bmatrix} d_{east}^2 & d_{EN} & d_{EV} & d_{ET} \\ d_{EN} & d_{north}^2 & d_{NV} & d_{NT} \\ d_{EV} & d_{NV} & d_V^2 & d_{VT} \\ d_{ET} & d_{NT} & d_{VT} & d_T^2 \end{bmatrix} \tag{C-4}$$

$$G(n\times 4) = \begin{bmatrix} -\cos E_1 \sin Az_1 & -\cos E_1 \cos Az_1 & -\sin E_1 & 1 \\ \cdots & \cdots & \cdots & \cdots \\ \cdots & \cdots & \cdots & \cdots \\ -\cos E_n \sin Az_n & -\cos E_n \cos Az_n & -\sin E_n & 1 \end{bmatrix} = \begin{bmatrix} u_1^T & 1 \\ \cdots & \cdots \\ \cdots & \cdots \\ u_n^t & 1 \end{bmatrix} \tag{C-5}$$

where E_i and Az_i are the elevation and azimuth angles between the receiver and the ith satellite, respectively.

If we assume that each of the error components in the east, north, and vertical directions is a normal distribution with zero mean, then the probability associated with the VPE equation shown in (C-1) is 0.9545. Also, the probability associated with the HPE equation ranges between 0.9545 when ($\frac{d_{\text{minor}}}{d_{major}} = 0$, e.g., the error ellipse becomes a straight line) and 0.982 (when $\frac{d_{\text{minor}}}{d_{major}} = 1$, e.g., the error ellipse becomes a circle) [11].

Calculation of the W-Matrix for dual-frequency user receiver:

For dual-frequency receivers for open sky users, no correlation of the ionosphere and troposphere was assumed, resulting in the following W-matrix:

$$W(n \times n) = R^{-1} = \begin{bmatrix} \frac{1}{\sigma_1^2} & 0 & \cdots & 0 \\ 0 & \frac{1}{\sigma_2^2} & \cdots & 0 \\ \vdots & \vdots & \ddots & \vdots \\ 0 & 0 & \cdots & \frac{1}{\sigma_n^2} \end{bmatrix} \qquad \text{(C-6)}$$

For dual-frequency receivers for urban users, partial correlation between satellites should be considered, resulting in the following W-matrix:

$$W(n \times n) = R^{-1}, \quad R = \begin{bmatrix} \sigma_1^2 & \rho_{12}\sigma_1\sigma_2 & \cdots & \rho_{1n}\sigma_1\sigma_n \\ \rho_{12}\sigma_1\sigma_2 & \sigma_2^2 & \cdots & \rho_{2n}\sigma_2\sigma_n \\ \vdots & \vdots & \ddots & \vdots \\ \rho_{1n}\sigma_1\sigma_n & \rho_{2n}\sigma_2\sigma_n & \cdots & \sigma_n^2 \end{bmatrix} \qquad \text{(C-7)}$$

In C-7, $\rho_{i,j}$ is the correlation between the i^{th} and j^{th} satellites. This correlation is related to the separation between satellites, however, the exact formulation of that relationship has not been determined. Therefore, we will assume a conservative approach and consider the correlation to be zero.

Calculation of the W-Matrix for single-frequency user receiver:

For single frequency user receivers, partial correlation of the ionosphere and full correlation of the troposphere are assumed as follows:

$$W = R^{-1}$$

where

$$R = R_{iono} + R_{tropo} + R_{clk\_ephem} + R_{multipath} + R_{noise}$$

$$R_{iono} = \begin{pmatrix} \sigma^2_{L1\_slant\_iono,1} & \rho_{iono}\sigma_{L1\_slant\_iono,1}\sigma_{L1\_slant\_iono,2} & & \\ \rho_{iono}\sigma_{L1\_slant\_iono,2}\sigma_{L1\_slant\_iono,1} & \cdots & & \\ & & \cdots & \\ & & & \sigma^2_{L1\_slant\_iono,n} \end{pmatrix}$$

$$R_{tropo} = \begin{pmatrix} \sigma^2_{slant\_tropo,1} & \rho_{tropo}\sigma_{slant\_tropo,1}\sigma_{slant\_tropo,2} & & \\ \rho_{tropo}\sigma_{slant\_tropo,2}\sigma_{slant\_tropo,1} & \cdots & & \\ & & \cdots & \\ & & & \sigma^2_{slant\_tropo,n} \end{pmatrix}$$

$$R_{clk\_ephem} = \begin{pmatrix} URE^2 & 0 & 0 & 0 \\ 0 & URE^2 & 0 & 0 \\ 0 & 0 & \cdots & \\ 0 & 0 & & URE^2 \end{pmatrix}$$

$$R_{multipath} = \begin{pmatrix} \sigma^2_{multipath,1} & 0 & 0 & 0 \\ 0 & \sigma^2_{multipath,2} & 0 & 0 \\ 0 & 0 & \cdots & \\ 0 & 0 & & \sigma^2_{multipath,n} \end{pmatrix},$$

$$R_{noise} = \begin{pmatrix} \sigma^2_{noise,1} & 0 & 0 & 0 \\ 0 & \sigma^2_{noise,2} & 0 & 0 \\ 0 & 0 & \cdots & \\ 0 & 0 & & \sigma^2_{noise,n} \end{pmatrix}$$

VPE and HPE Equations for Combined GPS and Galileo Constellations [5]

For the combined GPS and Galileo constellations, the observation matrix (G) is augmented as follows:

$$G(n+1\times 5)=\begin{bmatrix} G_{GPS}(n_{GPS}\times 5) \\ G_{Gal}(n_{Gal}\times 5) \\ 0 \quad 0 \quad 0 \quad 1 \quad -1 \end{bmatrix}$$

$n = n_{GPS} + n_{Gal}$ = total number of visible satellites

where:

$$G_{GPS}(n_{GPS}\times 5)=\begin{bmatrix} u^{T}_{GPS,1} & 1 & 0 \\ \cdots & \cdots & \cdots \\ \cdots & \cdots & \cdots \\ u^{T}_{GPS,n_{GPS}} & 1 & 0 \end{bmatrix},\ G_{Gal}(n_{Gal}\times 5)=\begin{bmatrix} u^{T}_{Gal,1} & 0 & 1 \\ \cdots & \cdots & \cdots \\ \cdots & \cdots & \cdots \\ u^{T}_{Gal,n_{Gal}} & 0 & 1 \end{bmatrix}$$

The covariance and W-matrices are calculated as follows:

$$C(5\times 5)=\left(\mathrm{G}^{T}\mathrm{WG}\right)^{-1},\quad W(n+1\times n+1)=\begin{bmatrix} & & 0 \\ & R^{-1}(n\times n) & 0 \\ & & \cdots \\ & & 0 \\ 0 \quad 0 & \cdots \quad 0 & \dfrac{1}{\sigma^{2}_{GGTO}} \end{bmatrix}$$

where:

σ_{GGTO} = GPS-Galileo Time Offset (converted to meters) = $2.5 \cdot 10^{-9} \cdot$ c (m) = 0.749481145 (m).

Using the above covariance matrix (C), the VPE and HPE for the combined GPS and Galileo constellations are calculated using Equation C-1.

Appendix D

Range Error Models for Single-and Dual-frequency Receivers in Open Sky and Urban Environments

D.1 **Dual-Frequency Error Model**

The dual-frequency user receiver error models are given by the following equations:

For Open Sky environment (E • 5°):

$$\sigma_{DF,opensky} = \sigma_{DF,iono-free,opensky} \tag{D-1}$$

For Urban Environment (E • 15°):

$$\sigma_{DF,urban} = \sigma_{DF,WLS} \tag{D-2}$$

D.1.1 **MBOC(L1/E1)/BPSK-R(10)(L5/E5a) GNSS Dual-Frequency User Error Model Using Iono-Free Combinations**

$$\sigma_{DF,iono-free} = \sigma_{L1C-L5} = \sqrt{URE^2 + \sigma^2_{tropo} + \sigma^2_{iono-free}} \tag{D-3}$$

where:

$$URE_{GPS} = 0.25m, URE_{Gal} = 0.7m$$

$$\sigma_{tropo} = (0.05m)\left(\frac{1.001}{\sqrt{0.002001 + \sin^2(E_i)}}\right)$$

$$\sigma^2_{iono-free} = \left(\frac{f_1^2}{f_1^2 - f_5^2}\right)^2 \sigma^2_{L1,air} + \left(\frac{f_5^2}{f_1^2 - f_5^2}\right)^2 \sigma^2_{L5,air} = \left(2.26\sigma_{L1,air}\right)^2 + \left(1.26\sigma_{L5,air}\right)^2$$

$$f_1 = 1575.42\ \text{MHz},\ f_5 = 1176.45\ \text{MHz} \tag{D-4}$$

$$\sigma_{L1,air} = \sqrt{RMS^2_{pr\_air,GPS} + \sigma^2_{L1,multipath}},$$

$$\sigma_{L5,air} = \sqrt{RMS^2_{pr\_air,GPS} + \sigma^2_{L5,multipath}}$$

$$RMS_{pr\_air,GPS} = 0$$

For Open Sky Environments (E • 5 degrees):

$$\sigma_{multipath,L1C,MBOC} = 0.070391 + 0.37408 \times \exp\left(-0.037694 E_i(\deg)\right)$$
$$\sigma_{multipath,L5(BPSK-10)} = 0.077988 + 0.32624 \times \exp\left(-0.036692 E_i(\deg)\right) \tag{D-5}$$

For Urban Environments (E • 15 degrees):

$$\sigma_{multipath,L1C,MBOC} = 3.368 - 2.1039 \times \text{atan}\left(0.71064\left(E(\text{deg}) - 28.78\right)\right)$$
$$\sigma_{multipath,L5(BPSK-10)} = 1.4874 - 0.93077 \times \text{atan}\left(0.3876\left(El_i(\text{deg}) - 27.88\right)\right) \quad \text{(D-6)}$$

D.1.2 **MBOC(L1/E1)/BPSK-R(10)(L5/E5a) GNSS Dual-Frequency User Error Model Using Weighted Least Squares (WLS)**

The WLS estimate of dual-frequency PR from the PR measurements at L1/E1 and L5/E5a is given by Jones et al. [10] as follows:

$$PR_{DF\_WLS} = \alpha_1 PR_{L1} + \alpha_2 PR_{L5}, \quad \alpha_1 + \alpha_2 = 1 \quad \text{(D-7)}$$

$$\alpha_1 = \frac{\sigma_{L5}^2 - \rho\sigma_{L1}\sigma_{L5}}{\sigma_{L5}^2 - 2\rho\sigma_{L1}\sigma_{L5} + \sigma_{L1}^2}$$
$$\alpha_2 = \frac{\sigma_{L1}^2 - \rho\sigma_{L1}\sigma_{L5}}{\sigma_{L5}^2 - 2\rho\sigma_{L1}\sigma_{L5} + \sigma_{L1}^2} \quad \text{(D-8)}$$

$$\sigma_{DF\_WLS}^2 = \frac{(1-\rho^2)\sigma_{L1}^2\sigma_{L5}^2}{\sigma_{L5}^2 - 2\rho\sigma_{L1}\sigma_{L5} + \sigma_{L1}^2} \quad \text{(D-9)}$$

where σ_{L1} and σ_{L5} are the error models for MBOC (L1/E1) and BPSK-R(10) (L5/E5a) single-frequency receivers and are given in Sections D.2 and D.3, respectively.

Estimating Variances and the Correlation Coefficient (r) between L1/E1 and L5/E5a signals:

The correlation matrix (R) between L1/E1 and L5/E5a signals is given as follows:

$$R = \begin{bmatrix} \sigma^2_{L1,iono} & \rho_{iono}\sigma_{L1,iono}\sigma_{L5,iono} \\ \rho_{iono}\sigma_{L1,iono}\sigma_{L5,iono} & \sigma^2_{L5,iono} \end{bmatrix} + \begin{bmatrix} \sigma^2_{L1,MP} & \rho_{MP}\sigma_{L1,MP}\sigma_{L5,MP} \\ \rho_{MP}\sigma_{L1,MP}\sigma_{L5,MP} & \sigma^2_{L5,MP} \end{bmatrix}$$
$$+ \begin{bmatrix} \sigma^2_{L1,tropo} & \rho_{tropo}\sigma_{L1,tropo}\sigma_{L5,tropo} \\ \rho_{tropo}\sigma_{L1,tropo}\sigma_{L5,tropo} & \sigma^2_{L5,tropo} \end{bmatrix}$$
$$+ \begin{bmatrix} \sigma^2_{L1,clock+eph} & \rho_{clock+eph}\sigma_{L1,clock+eph}\sigma_{L5,clock+eph} \\ \rho_{clock+eph}\sigma_{L1,clock+eph}\sigma_{L5,clock+eph} & \sigma^2_{L5,clock+eph} \end{bmatrix} + \begin{bmatrix} \sigma^2_{L1,noise} & 0 \\ 0 & \sigma^2_{L5,noise} \end{bmatrix}$$
$$= \begin{bmatrix} \sigma^2_{L1} & \rho\sigma_{L1}\sigma_{L5} \\ \rho\sigma_{L1}\sigma_{L5} & \sigma^2_{L5} \end{bmatrix}$$

$$\sigma^2_{L1} = \sigma^2_{L1,iono} + \sigma^2_{L1,MP} + \sigma^2_{L1,tropo} + \sigma^2_{L1,clock+eph} + \sigma^2_{L1,noise}$$

$$\sigma^2_{L5} = \sigma^2_{L5,iono} + \sigma^2_{L5,MP} + \sigma^2_{L5,tropo} + \sigma^2_{L5,clock+eph} + \sigma^2_{L5,noise}$$

$$\rho\sigma_{L1}\sigma_{L5} = \rho_{iono}\sigma_{L1,iono}\sigma_{L5,iono} + \rho_{MP}\sigma_{L1,MP}\sigma_{L5,MP} + \rho_{tropo}\sigma_{L1,tropo}\sigma_{L5,tropo}$$
$$+ \rho_{clock+eph}\sigma_{L1,clock+eph}\sigma_{L5,clock+eph} + \rho_{noise}\sigma_{L1,noise}\sigma_{L5,noise}$$

$$\rho = \frac{\rho_{iono}\sigma_{L1,iono}\sigma_{L5,iono} + \rho_{tropo}\sigma_{L1,tropo}\sigma_{L5,tropo} + \rho_{clock+eph}\sigma_{L1,clock+eph}\sigma_{L5,clock+eph}}{\sigma_{L1}\sigma_{L5}}$$

where we assume

$$\rho_{iono} = 1.0, \quad \rho_{MP} = 0, \quad \rho_{tropo} = 1.0, \quad \rho_{clock+eph} = 1.0, \quad \rho_{noise} = 0.0$$

$$W = R^{-1} = \frac{1}{(1-\rho^2)\sigma^2_{L1}\sigma^2_{L5}} \begin{bmatrix} \sigma^2_{L5} & -\rho\sigma_{L1}\sigma_{L5} \\ -\rho\sigma_{L1}\sigma_{L5} & \sigma^2_{L1} \end{bmatrix}$$

$$\text{Covariance Matrix} = C = \left(G^T W G\right)^{-1}, G = \begin{bmatrix} 1 \\ 1 \end{bmatrix}$$

$$C = \sigma^2_{DF\_WLS} = \frac{(1-\rho^2)\sigma^2_{L1}\sigma^2_{L5}}{\sigma^2_{L5} - 2\rho\sigma_{L1}\sigma_{L5} + \sigma^2_{L1}}$$

Note: This result is consistent with that of Jones et al. [10].

D.2 **BOC(1,1) and MBOC (L1/E1) GNSS Single-Frequency User Error Model**

$$\sigma_{L1} = \sqrt{URE^2 + \sigma_{tropo}^2 + \sigma_{L1,iono}^2 + \sigma_{L1,air}^2}$$

$$URE_{GPS} = 0.25m, URE_{Gal} = 0.7m$$

$$\sigma_{tropo} = (0.05m)\left(\frac{1.001}{\sqrt{0.002001 + \sin^2(E)}}\right)$$

$$\sigma_{L1,air} = \sqrt{RMS_{pr\_air,GPS}^2 + \sigma_{L1,multipath}^2},$$

$$RMS_{pr\_air,GPS} = 0.0$$

For Open Sky Environments ($E \geq 5^0$):

$$\sigma_{multipath,L1C-MBOC} = 0.070391 + 0.37408 \times \exp(-0.037694 \times E(\deg))$$

$$\sigma_{multipath,L1C-BOC(1,1)} = 0.22176 + 2.2128 \times \exp(-0.057807 \times E(\deg))$$

For Urban Environments ($E \geq 15^0$):

$$\sigma_{multipath,L1C-MBOC} = 3.368 - 2.1039 \times \operatorname{atan}(0.71064 \times (E(\deg) - 28.78))$$

$$\sigma_{multipath,L1C-BOC(1,1)} = 6.6798 - 4.2324 \times \operatorname{atan}(0.35457 \times (E(\deg) - 27.77))$$

$$\sigma_{L1,iono} = kT_{iono}$$

$$k = \begin{cases} 0.25, & \text{minimum solar cycle} \\ 0.4, & \text{average solar cycle} \\ 0.29, & \text{peak solar cycle} \end{cases}$$

T_{iono} = slant ionospheric delay calculated by the single - frequency model (IS - GPS - 200E)

D.3 **BPSK-R(10) (L5/E5a) GNSS Single-Frequency User Error Model**

$$\sigma_{L5} = \sqrt{URE^2 + \sigma_{tropo}^2 + \sigma_{L5,iono}^2 + \sigma_{L5,air}^2}$$

$$URE_{GPS} = 0.25m, URE_{Gal} = 0.7m$$

$$\sigma_{tropo} = (0.05m)\left(\frac{1.001}{\sqrt{0.002001 + \sin^2(E)}}\right)$$

$$\sigma_{L5,air} = \sqrt{RMS_{pr\_air,GPS}^2 + \sigma_{L5,multipath}^2}$$

$$RMS_{pr\_air,GPS} = 0.0$$

Open Sky ($E \geq 5^0$):

$$\sigma_{multipath,L5-BPSK-R10} = 0.077988 + 0.32624\exp(-0.036692 * E(\deg))$$

Urban ($E \geq 15^0$):

$$\sigma_{multipath,L5-BPSK-R10} = 1.4874 - 0.93077 * \text{atan}(0.3876 * (E(\deg) - 27.88))$$

$$\sigma_{L5,iono} = \left(\frac{f_{L1}^2}{f_{L5}^2}\right)\sigma_{L1,iono} = 1.7933\sigma_{L1,iono}$$

$$\sigma_{L1,iono} = kT_{iono}$$

$$k = \begin{cases} 0.25, & \text{minimum solar cycle} \\ 0.4, & \text{average solar cycle} \\ 0.29, & \text{peak solar cycle} \end{cases}$$

T_{iono} = slant ionospheric delay calculated by the single - frequency model (IS - GPS - 200E)

D.4 **An Example of a Total Urban Error Model for Guayaquil, Ecuador (Average Ionosphere):**

Figures D-1 and D-2 show the urban error models for Guayaquil, Ecuador (Average Ionosphere) at 4:00 AM and 2:00 PM local time, respectively. Each of these figures shows two subplots. The top subplot shows the error models for:

a) DF L1C-MBOC/L5 (iono-free),
b) SF L1C-MBOC,
c) SF L1C-BOC(1,1),
d) SF L5-BPSK-R(10), and
e) DF-WLS.

The bottom subplot shows the correlation coefficient between L1/E1 and L5/E5a signals.

The top subplot shows that DF-WLS (magenta curve) is the smallest error model and would represent the effects of a reasonable multipath mitigation technique for urban environments.

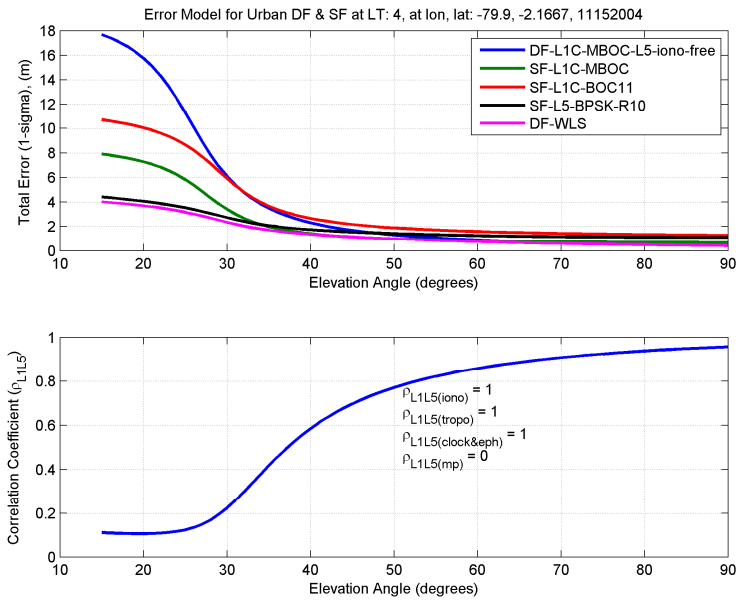

Figure D-1 Total Urban Error Model for Guayaquil, Ecuador (Average Ionosphere) (Local Time: 4:00AM)

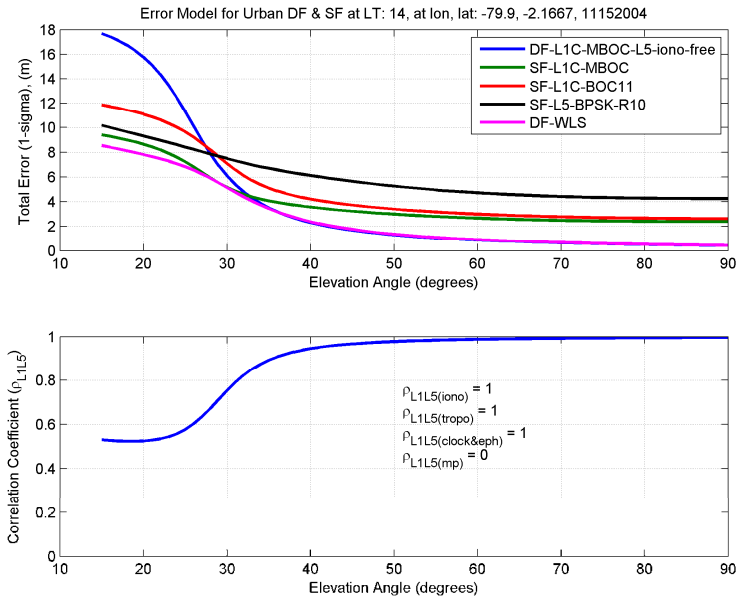

Figure D-2 Total Urban Error Model for Guayaquil, Ecuador (Average Ionosphere) (Local Time: 2:00PM)

Appendix E

Summary of Validation Results

E.1 Validation of Accuracy Model

The goal is to produce VPE and HPE estimates which are close to the values published in the FAA GPS Performance Analysis (PAN) reports [4]. The following three days were selected to represent the solar cycle:

- March 15, 2009, representative of minimum solar cycle,
- November 15, 2004, representative of the average solar cycle, and
- November 15, 2002, representative of the Peak solar cycle.

This selection is based on the 3-month average of SSN and F10.7 over 11-year Cycle shown in Figure E-1.

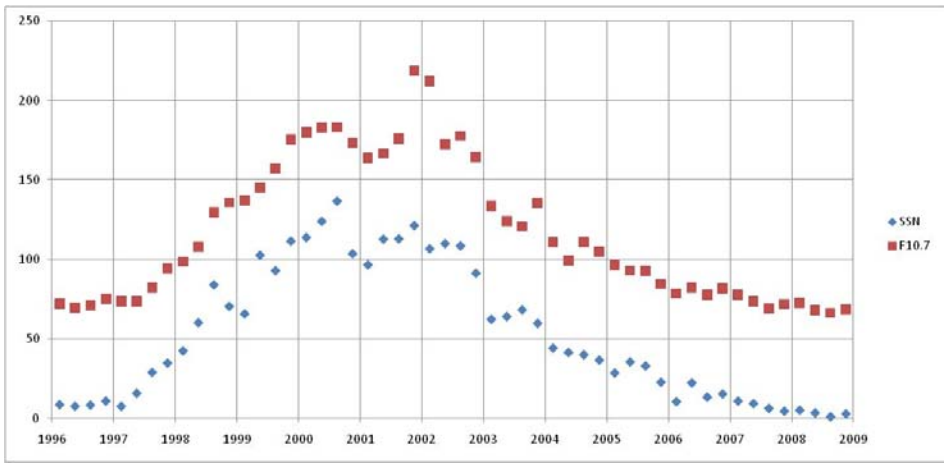

Figure E-1. 3-month average of SSN and F10.7 Over 11-year Cycle

E-2 Assumptions used in the Model Validation

The Klobuchar coefficients (• 's and • 's) were obtained from the RINEX navigation files for these three days. For validation purposes only, the following assumptions were used in order to reasonably match the PAN values:

- Actual GPS constellation for each of the 3 representative days
- Signal: L1C/A
- URE = 0.8
- For single-frequency, the ionospheric error = $\sigma_{UIRE} = k*T_{iono}$
  - k = a parameter such that $0 < k \bullet 1$
  - T_{iono} = slant ionospheric delay in meters from single-frequency correction model
- Correlation for ionosphere and troposphere was included (see Appendix C)
- Multipath open sky model for L1/CA
  - $s_{mp} = 0.067 + 0.426e^{-0.043E}$ for BPSK-R(1) 24 MHZ

where E is the elevation angle in degrees [2].

E-3 Summary of Validation Results

Table B-1 shows the summary of validation results.

Table E-1. Summary of Validation Results

	Minimum (without Iqaluit)	Average (without Mauna Loa and Honolulu)	Peak
Date Selected	**March 15, 2009**	**November 15, 2004**	**November 15, 2002**
Number of sites	**26**	**19**	**13**
k	0.25	0.40	0.29
rho_iono	0.80	0.75	0.80
rho_tropo	1.00	1.00	1.00
Mean (HPE), PAN Report (m)	2.255	2.979	5.078
Mean (HPE), MITRE (m)	2.264	2.961	5.134
Mean(VPE), PAN Report (m)	4.556	5.826	12.413
Mean (VPE), MITRE(m)	4.556	5.888	12.197
Percentage Position Difference	**0.18%**	**0.99%**	**1.66%**
Max HPE (m) (MITRE)	2.528	3.568	5.566
Max VPE (m) (MITRE)	5.890	**8.302**	12.987

E-4 Recommendation of the Validation Process

Based on the validation study, the following parameters are used in the analysis of this report:

- Minimum Solar Cycle: k = 0.25, $\bullet_{iono}$ = 0.80,
- Average Solar Cycle: k = 0.40, $\bullet_{iono}$ = 0.75, and
- Peak of Solar Cycle: k = 0.29, $\bullet_{iono}$ = 0.80.

The scale factor *k* should directly multiply the computed slant delay, while the correlation coefficient applies to the non-diagonal terms of the covariance matrix used for the computation of the Horizontal Position Error (HPE) and Vertical Position Error (VPE) (see Appendix C).

Appendix F

Complete Results for the Principal Study

This appendix contains all results for the three ionospheric solar cycle days and other figures not presented in the core part of the note. This includes the maps of mean VPE/HPE, the tables of statistics of mean VPE/HPE, and the empirical CDFs of VPE and HPE.

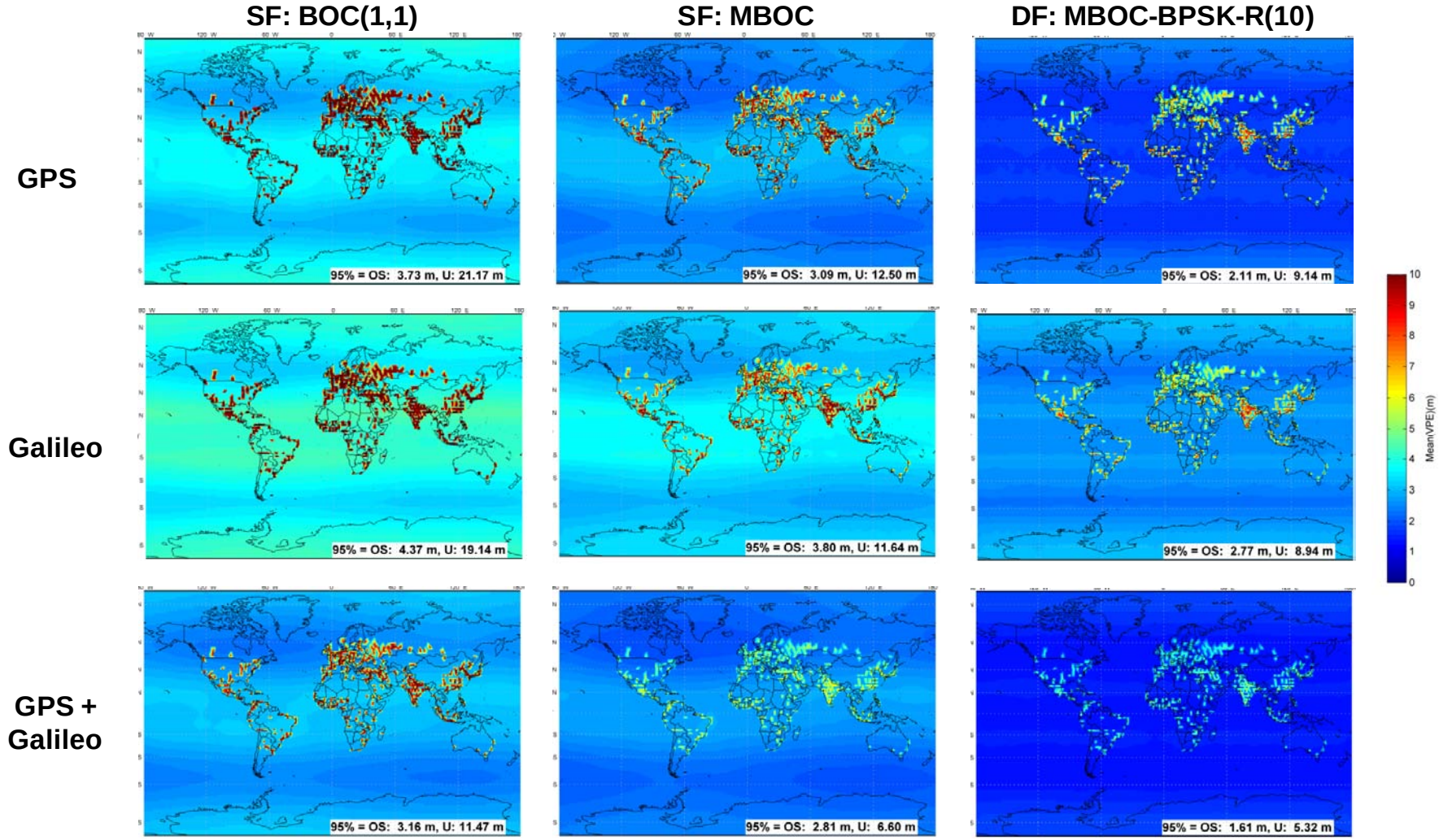

Figure F-1: Comparison of Mean VPE(m) for Minimum Solar Cycle

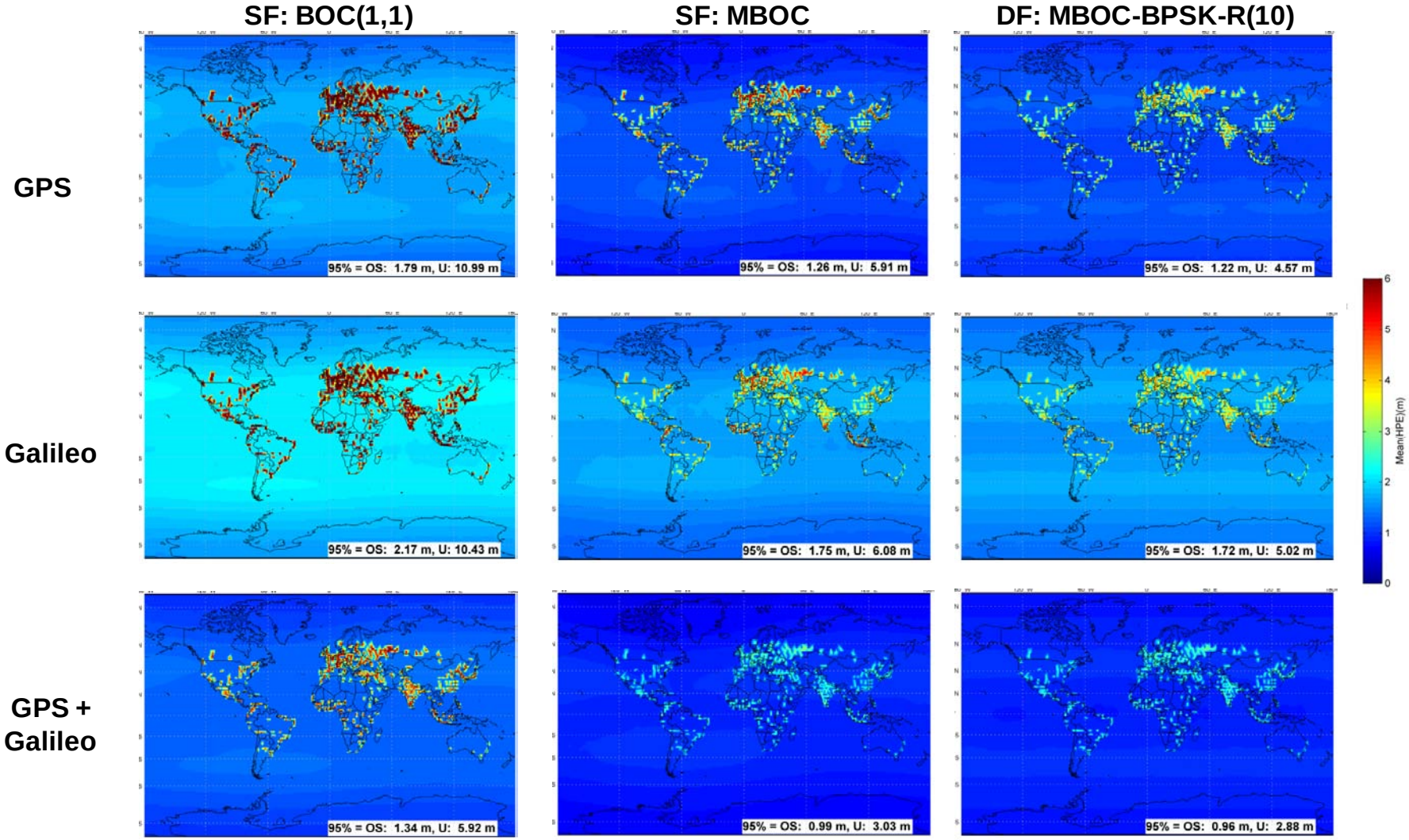

Figure F-2: Comparison of Mean HPE(m) for Minimum Solar Cycle

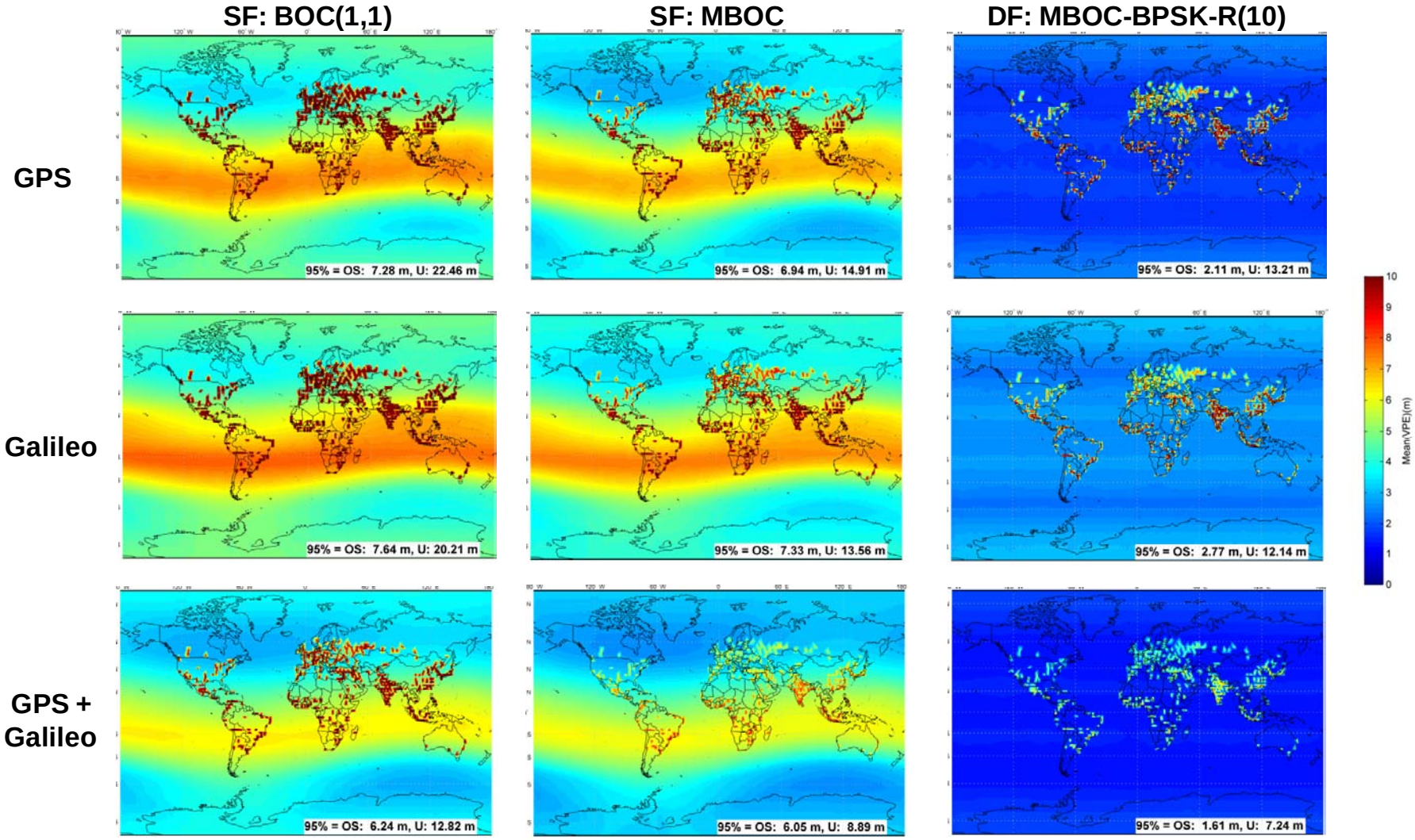

Figure F-3: Comparison of Mean VPE(m) for Average Solar Cycle

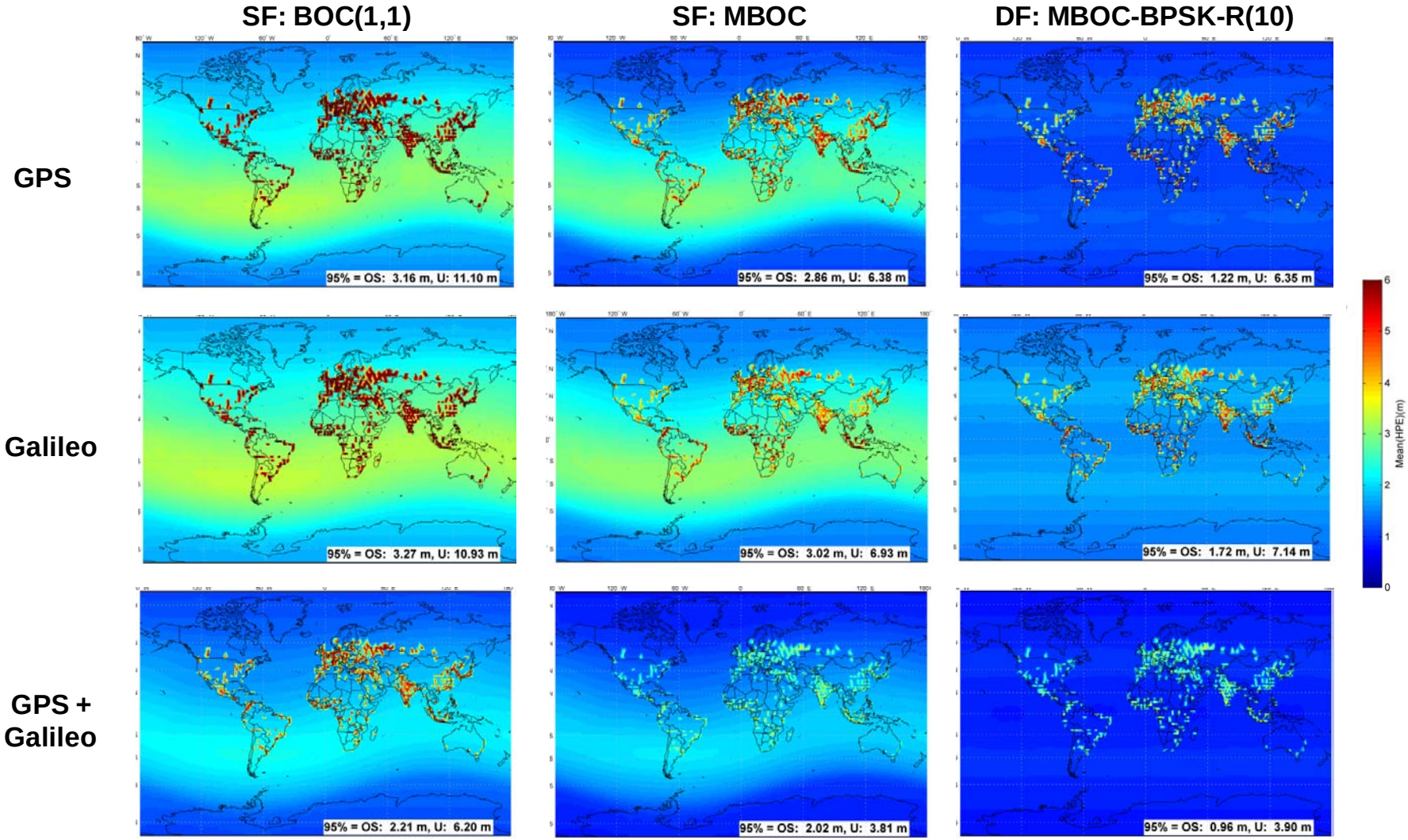

Figure F-4: Comparison of Mean HPE(m) for Average Solar Cycle

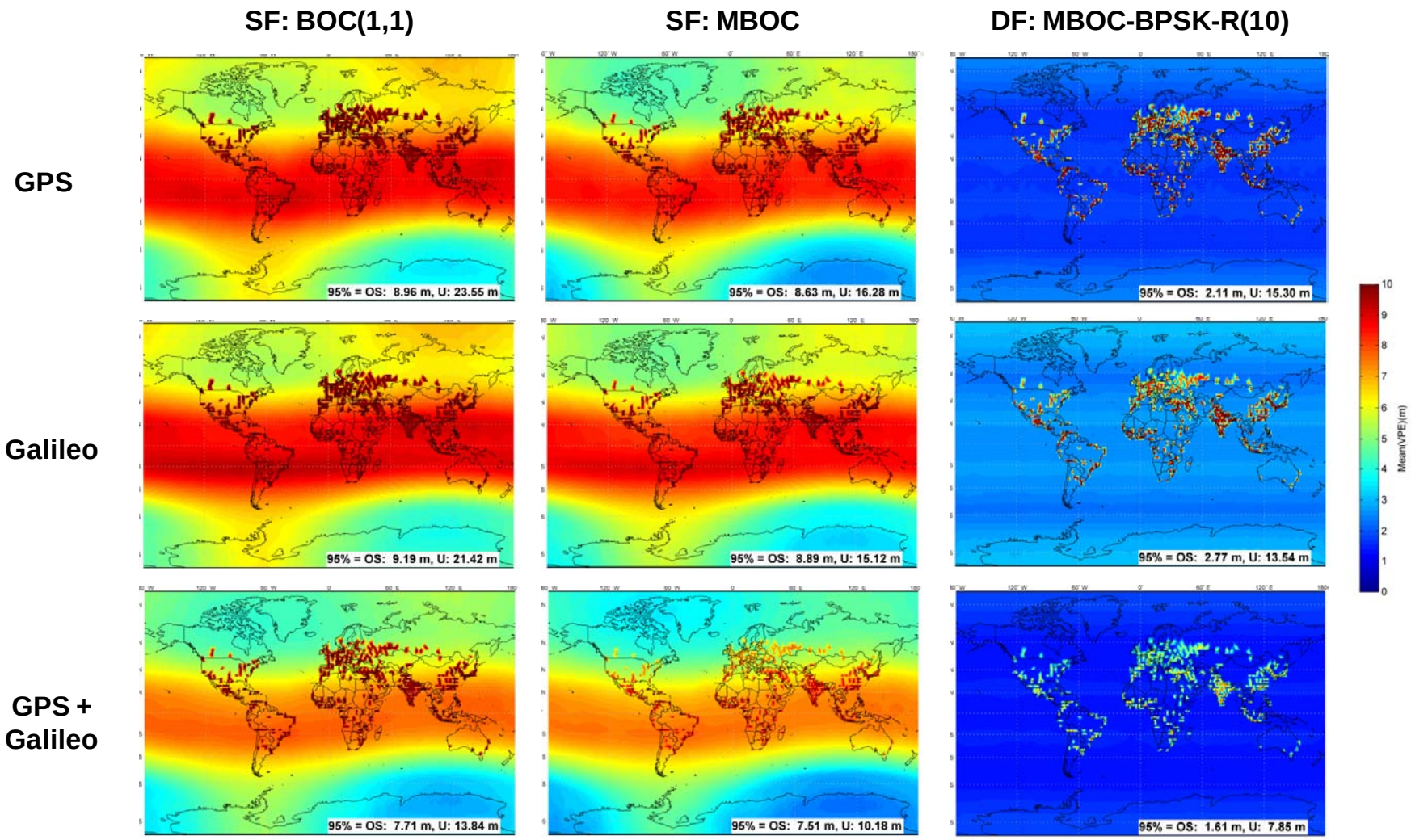

Figure F-5: Comparison of Mean VPE(m) for Peak Solar Cycle

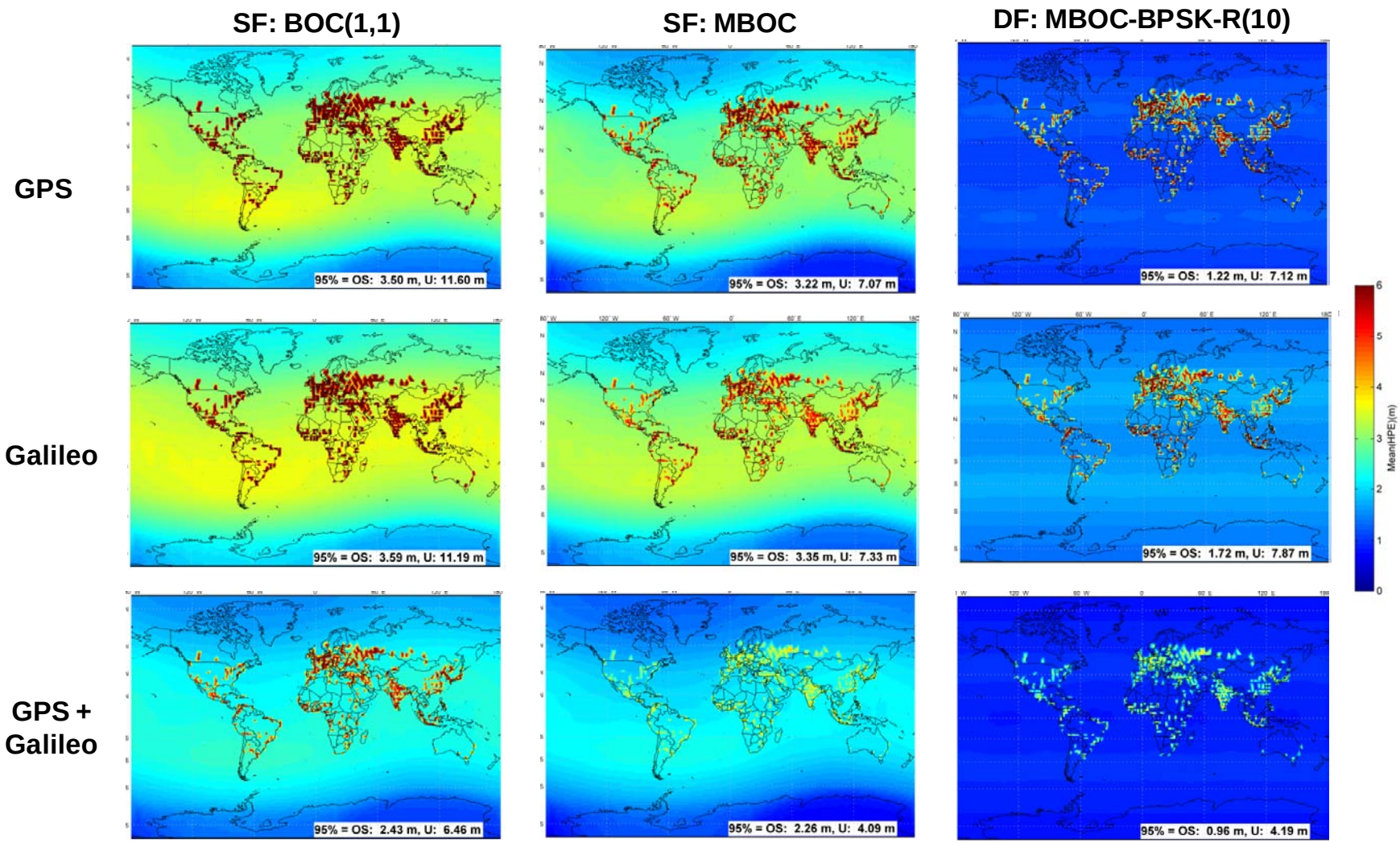

Figure F-6: Comparison of Mean HPE(m) for Peak Solar Cycle

Table F-1: Global Statistics of Mean VPE(m) and HPE(m) for Minimum Solar Cycle

VPE

		SF: BOC(1,1)		SF: MBOC		DF: MBOC-BPSK10	
	VPE	Open Sky	Urban	Open Sky	Urban	Open Sky	Urban
GPS	%ge pdop = 10 & nsat = 4	100%	99.42%	100%	99.42%	100%	99.42%
	mean	3.39	18.89	2.73	10.65	1.76	7.93
	stdev	0.29	1.57	0.31	1.29	0.15	0.79
	RMS	3.40	18.96	2.74	10.72	1.76	7.97
	Median	3.49	19.05	2.79	10.61	1.73	8.08
	95th	3.73	21.17	3.09	12.50	2.11	9.14
Galileo	%ge pdop = 10 & nsat = 4	100%	100%	100%	100%	100%	100%
	mean	3.95	16.78	3.41	10.07	2.58	7.81
	stdev	0.33	1.59	0.32	1.00	0.14	0.83
	RMS	3.97	16.85	3.42	10.12	2.58	7.85
	Median	4.09	16.68	3.53	9.95	2.56	7.87
	95th	4.37	19.14	3.80	11.64	2.77	8.94
GPS & Galileo	%ge pdop = 10 & nsat = 4	100%	100%	100%	100%	100%	100%
	mean	2.86	10.78	2.48	6.03	1.39	4.90
	stdev	0.26	0.54	0.28	0.44	0.10	0.34
	RMS	2.88	10.79	2.50	6.04	1.39	4.91
	Median	2.95	10.94	2.55	6.12	1.37	4.99
	95th	3.16	11.47	2.81	6.60	1.61	5.32

HPE

		SF: BOC(1,1)		SF: MBOC		DF: MBOC-BPSK10	
	HPE	Open Sky	Urban	Open Sky	Urban	Open Sky	Urban
GPS	%ge pdop = 10 & nsat = 4	100%	99.42%	100%	99.42%	100%	99.42%
	mean	1.67	9.43	1.14	4.93	1.13	4.24
	stdev	0.09	0.63	0.10	0.43	0.06	0.17
	RMS	1.68	9.45	1.14	4.95	1.14	4.24
	Median	1.68	9.23	1.16	4.80	1.13	4.22
	95th	1.79	10.99	1.26	5.91	1.22	4.57
Galileo	%ge pdop = 10 & nsat = 4	100%	100%	100%	100%	100%	100%
	mean	2.06	8.40	1.62	4.67	1.62	4.29
	stdev	0.11	1.02	0.11	0.68	0.08	0.34
	RMS	2.07	8.46	1.63	4.72	1.62	4.30
	Median	2.09	8.00	1.65	4.38	1.63	4.19
	95th	2.17	10.43	1.75	6.08	1.72	5.02
GPS & Galileo	%ge pdop = 10 & nsat = 4	100%	100%	100%	100%	100%	100%
	mean	1.26	5.33	0.91	2.67	0.90	2.69
	stdev	0.06	0.33	0.07	0.19	0.04	0.11
	RMS	1.26	5.34	0.91	2.68	0.90	2.69
	Median	1.27	5.23	0.92	2.61	0.90	2.68
	95th	1.34	5.92	0.99	3.03	0.96	2.88

Table F-2: Global Statistics of Mean VPE(m) and HPE(m) for Average Solar Cycle

VPE

		SF: BOC(1,1)		SF: MBOC		DF: MBOC-BPSK10	
	VPE	Open Sky	Urban	Open Sky	Urban	Open Sky	Urban
GPS	%ge pdop = 10 & nsat = 4	100%	99.42%	100%	99.42%	100%	99.42%
	mean	5.61	19.74	5.17	12.21	1.76	10.45
	stdev	1.27	1.92	1.36	1.85	0.15	1.83
	RMS	5.76	19.83	5.34	12.35	1.76	10.61
	Median	5.77	19.97	5.35	12.50	1.73	10.38
	95th	7.28	22.46	6.94	14.91	2.11	13.21
Galileo	%ge pdop = 10 & nsat = 4	100%	100%	100%	100%	100%	100%
	mean	5.91	17.58	5.55	11.39	2.58	9.80
	stdev	1.26	1.88	1.31	1.53	0.14	1.59
	RMS	6.05	17.68	5.70	11.49	2.58	9.93
	Median	6.11	17.60	5.74	11.71	2.56	10.11
	95th	7.64	20.21	7.33	13.56	2.77	12.14
GPS & Galileo	%ge pdop = 10 & nsat = 4	100%	100%	100%	100%	100%	100%
	mean	4.76	11.58	4.50	7.38	1.39	6.14
	stdev	1.12	0.92	1.18	1.04	0.10	0.77
	RMS	4.89	11.62	4.66	7.46	1.39	6.19
	Median	4.89	11.81	4.64	7.42	1.37	6.19
	95th	6.24	12.82	6.05	8.89	1.61	7.24

HPE

		SF: BOC(1,1)		SF: MBOC		DF: MBOC-BPSK10	
	HPE	Open Sky	Urban	Open Sky	Urban	Open Sky	Urban
GPS	%ge pdop = 10 & nsat = 4	100%	99.42%	100%	99.42%	100%	99.42%
	mean	2.56	9.81	2.20	5.66	1.13	5.50
	stdev	0.45	0.56	0.52	0.42	0.06	0.48
	RMS	2.60	9.82	2.26	5.68	1.14	5.52
	Median	2.64	9.64	2.31	5.62	1.13	5.43
	95th	3.16	11.10	2.86	6.38	1.22	6.35
Galileo	%ge pdop = 10 & nsat = 4	100%	100%	100%	100%	100%	100%
	mean	2.78	8.74	2.47	5.26	1.62	5.34
	stdev	0.42	1.05	0.46	0.76	0.08	0.76
	RMS	2.81	8.80	2.51	5.31	1.62	5.39
	Median	2.88	8.34	2.57	5.03	1.63	5.01
	95th	3.27	10.93	3.02	6.93	1.72	7.14
GPS & Galileo	%ge pdop = 10 & nsat = 4	100%	100%	100%	100%	100%	100%
	mean	1.84	5.60	1.61	3.19	0.90	3.33
	stdev	0.30	0.33	0.34	0.29	0.04	0.27
	RMS	1.87	5.61	1.64	3.21	0.90	3.34
	Median	1.91	5.50	1.69	3.09	0.90	3.24
	95th	2.21	6.20	2.02	3.81	0.96	3.90

Table F-3: Global Statistics of Mean VPE(m) and HPE(m) for Peak Solar Cycle

VPE

		SF: BOC(1,1)		SF: MBOC		DF: MBOC - BPSK10	
	VPE	Open Sky	Urban	Open Sky	Urban	Open Sky	Urban
GPS	%ge pdop = 10 & nsat = 4	100%	99.42%	100%	99.42%	100%	99.42%
	mean	7.49	21.00	7.05	14.11	1.76	12.48
	stdev	1.39	1.84	1.51	1.66	0.15	1.75
	RMS	7.62	21.08	7.21	14.20	1.76	12.60
	Median	7.94	21.33	7.57	14.30	1.73	12.54
	95th	8.96	23.55	8.63	16.28	2.11	15.30
Galileo	%ge pdop = 10 & nsat = 4	100%	100%	100%	100%	100%	100%
	mean	7.68	18.79	7.33	13.09	2.58	11.47
	stdev	1.42	1.86	1.49	1.44	0.14	1.55
	RMS	7.81	18.88	7.48	13.17	2.58	11.58
	Median	8.29	18.81	7.95	13.28	2.56	11.64
	95th	9.19	21.42	8.89	15.12	2.77	13.54
GPS & Galileo	%ge pdop = 10 & nsat = 4	100%	100%	100%	100%	100%	100%
	mean	6.39	12.84	6.10	9.11	1.39	7.03
	stdev	1.29	0.86	1.39	0.89	0.10	0.66
	RMS	6.52	12.87	6.25	9.16	1.39	7.06
	Median	6.83	13.18	6.59	9.34	1.37	7.17
	95th	7.71	13.84	7.51	10.18	1.61	7.85

HPE

		SF: BOC(1,1)		SF: MBOC		DF: MBOC - BPSK10	
	HPE	Open Sky	Urban	Open Sky	Urban	Open Sky	Urban
GPS	%ge pdop = 10 & nsat = 4	100%	99.42%	100%	99.42%	100%	99.42%
	mean	3.12	10.27	2.80	6.39	1.13	6.35
	stdev	0.40	0.56	0.46	0.33	0.06	0.46
	RMS	3.15	10.28	2.83	6.40	1.14	6.36
	Median	3.26	10.11	2.97	6.35	1.13	6.35
	95th	3.50	11.60	3.22	7.07	1.22	7.12
Galileo	%ge pdop = 10 & nsat = 4	100%	100%	100%	100%	100%	100%
	mean	3.27	9.15	2.99	5.88	1.62	5.98
	stdev	0.39	0.99	0.42	0.67	0.08	0.85
	RMS	3.30	9.21	3.02	5.92	1.62	6.04
	Median	3.43	8.76	3.17	5.62	1.63	5.66
	95th	3.59	11.19	3.35	7.33	1.72	7.87
GPS & Galileo	%ge pdop = 10 & nsat = 4	100%	100%	100%	100%	100%	100%
	mean	2.21	5.92	2.00	3.68	0.90	3.63
	stdev	0.25	0.31	0.29	0.20	0.04	0.27
	RMS	2.23	5.93	2.02	3.69	0.90	3.64
	Median	2.31	5.84	2.11	3.64	0.90	3.56
	95th	2.43	6.46	2.26	4.09	0.96	4.19

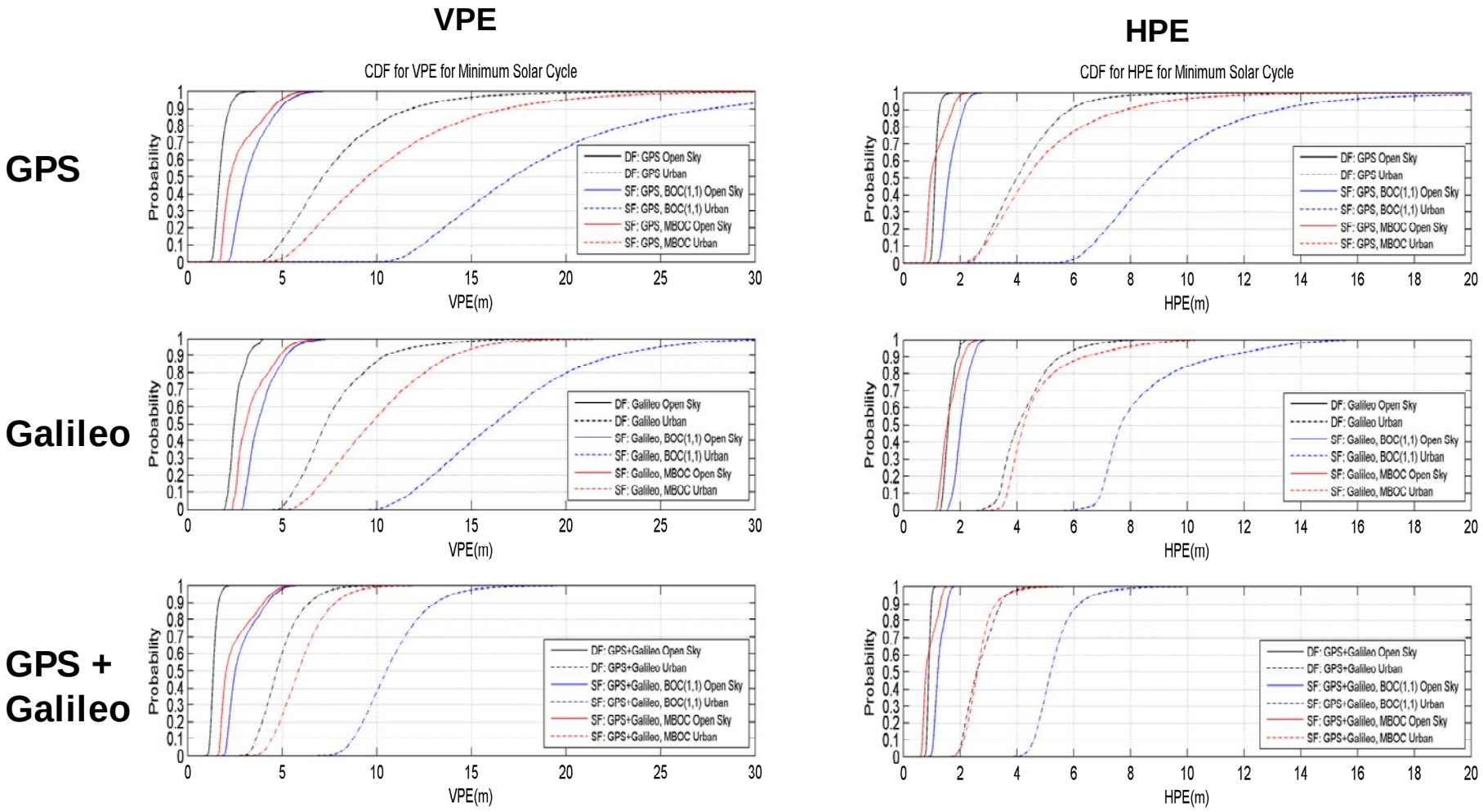

Figure F-7: Empirical CDFs of All Values of VPE and HPE for Minimum Solar Cycle

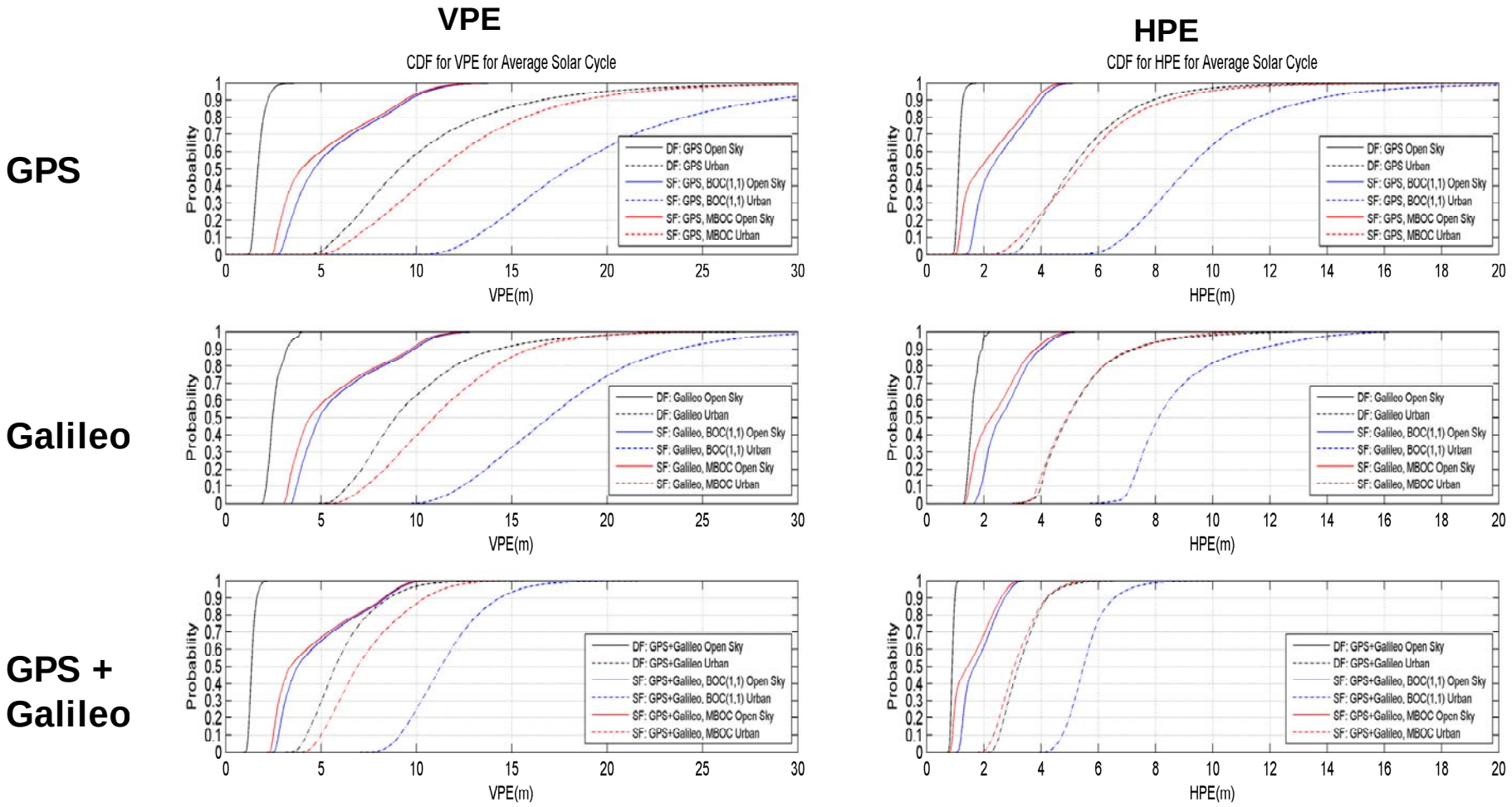

Figure F-8: Empirical CDFs of All Values of VPE and HPE for Average Solar Cycle

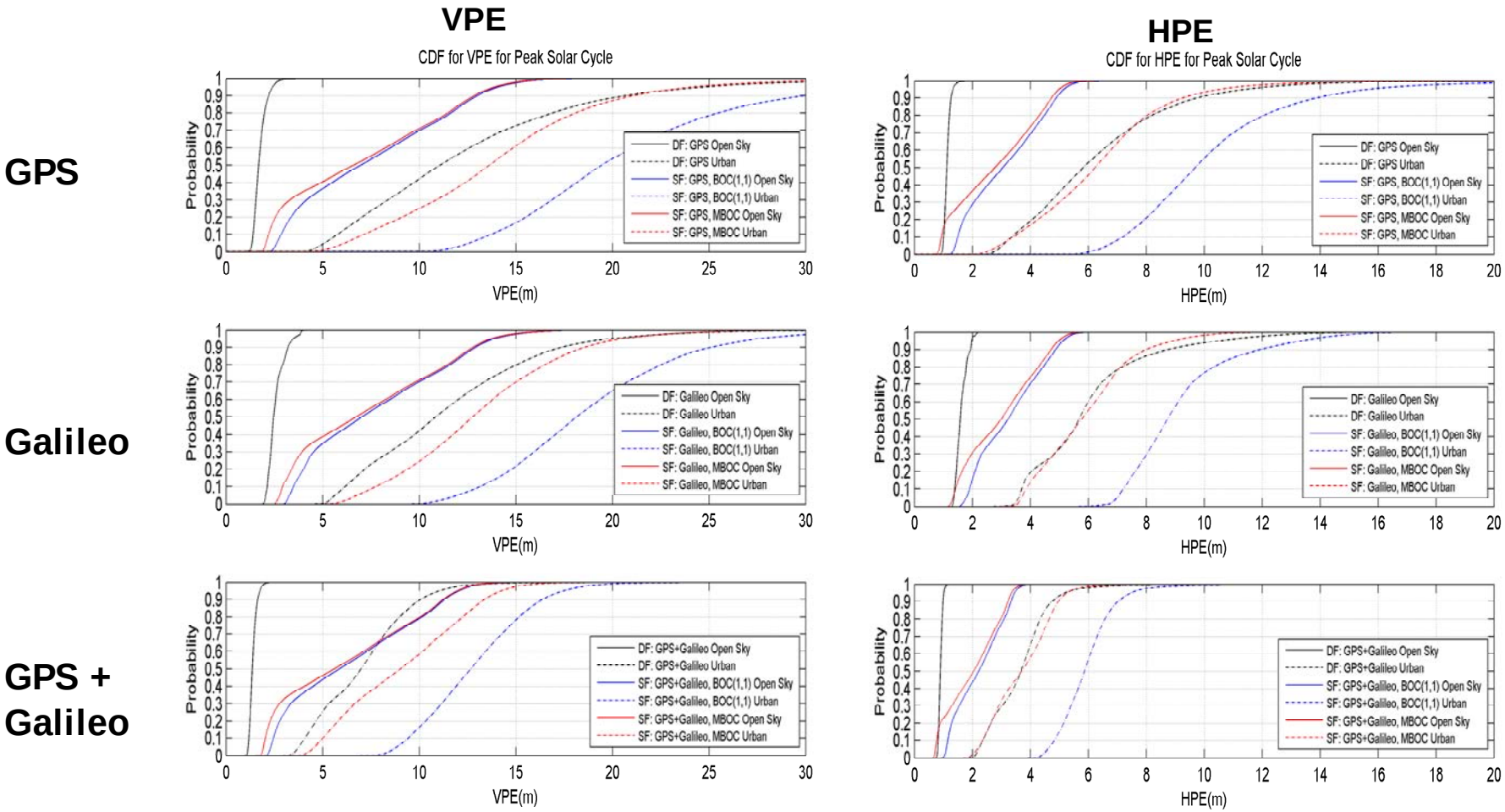

Figure F9: Empirical CDFs of All Values of VPE and HPE for Peak Solar Cycle

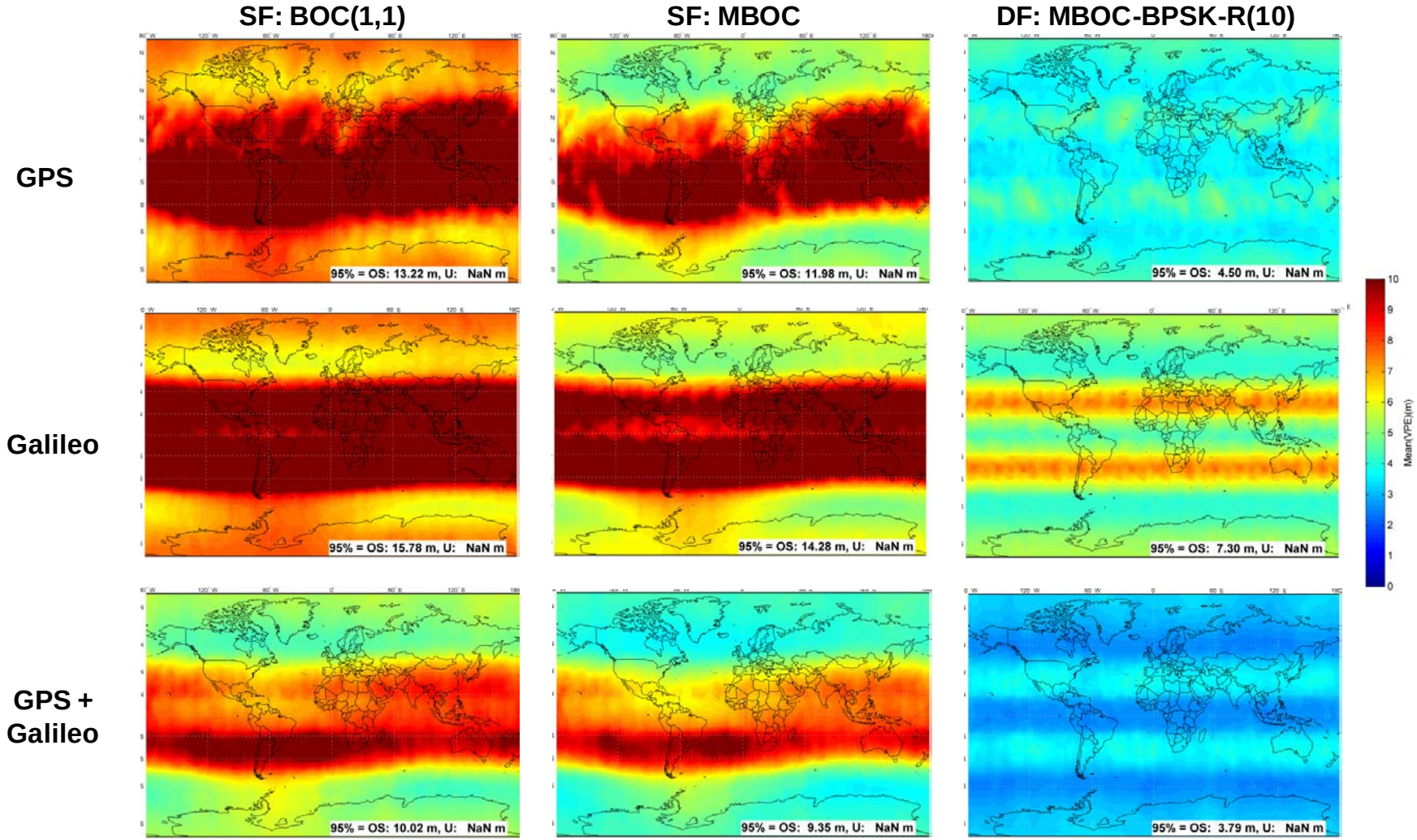

Figure F10: Half-Sky Study - Comparison of Half Sky Mean VPE(m) for Average Solar Cycle

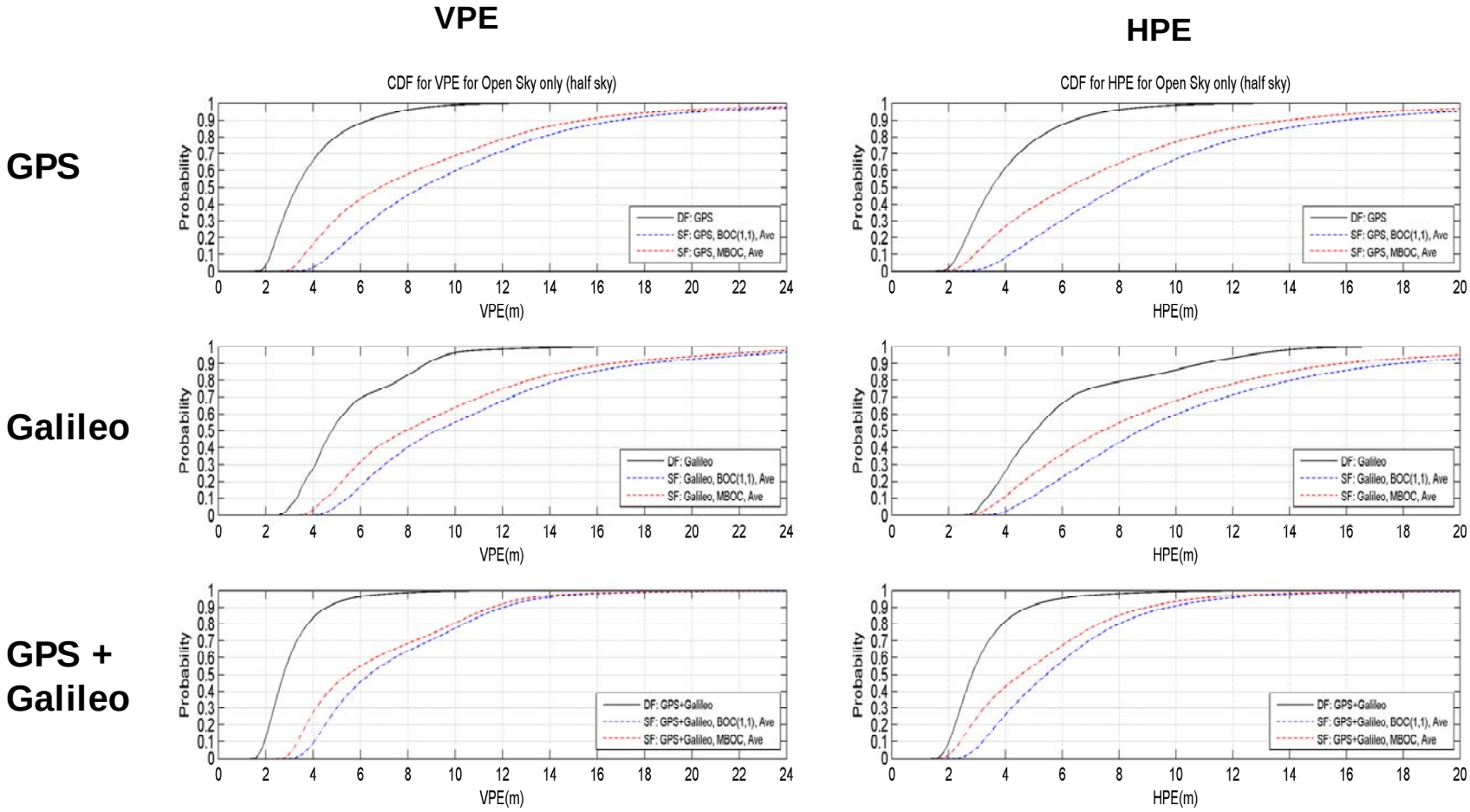

Figure F11: Half-Sky Study - Half Sky Empirical CDFs of All Values of VPE and HPE for Average Solar Cycle

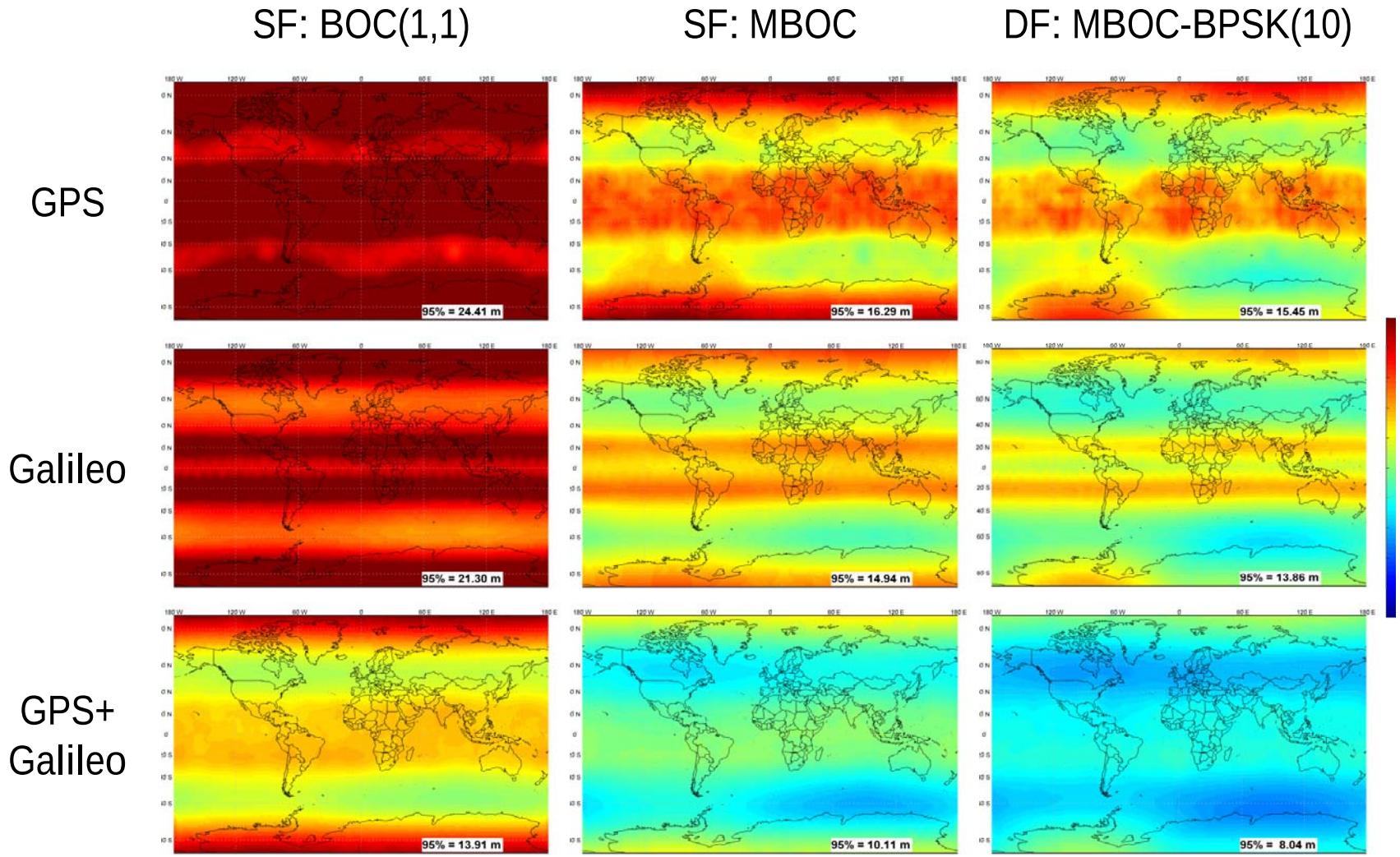

Figure F12: Urban Global Study (15º) - Comparison of Mean VPE(m) for Urban Global Study (15º) for Peak Solar Cycle

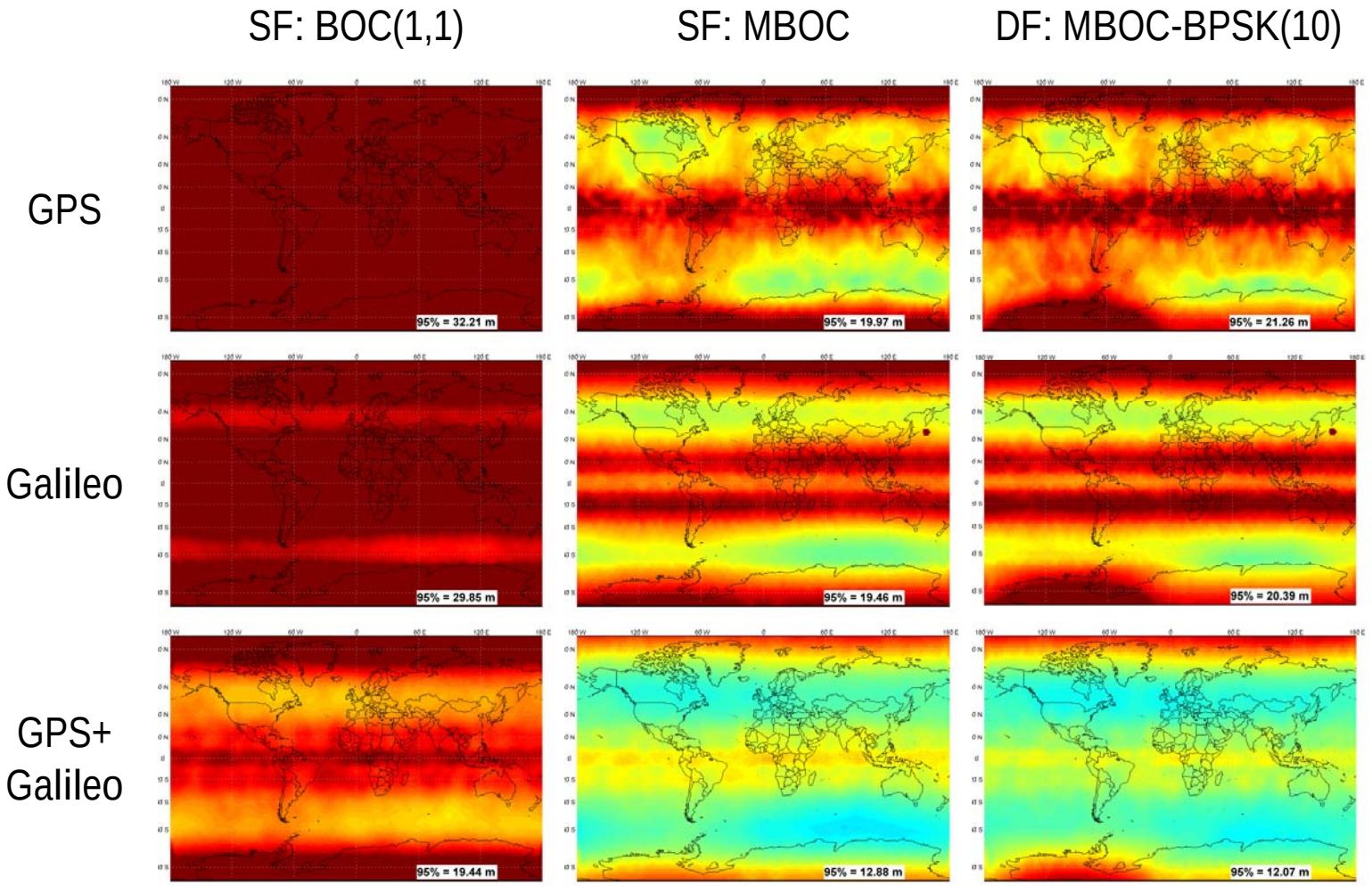

Figure F13: Urban Global Study (30º) - Comparison of Mean VPE(m) with 30° Mask Angle for Urban Global Study (30º) for Peak Solar Cycle

Appendix G

References

[1] RTCA, Inc. WAAS MOPS, DO-229D, Washington D.C., December 6, 2006.

[2] Hegarty, C., M. Tran, J. Betz, "Multipath Performance of the New GNSS Signals," ION-NTM-2004.

[3] Tran, M., "Multipath Models for L1-BPSK-10, MBOC(1,1) and BOC(1,1)', White Paper, MITRE/CAASD, July 24, 2009.

[4] http://www.nstb.tc.faa.gov/DisplayArchive.htm

[5] Blanch, J., "Including the Broadcast Time Difference in a joint GPS-Galileo Position Solution," white paper, Stanford University, July 15, 2009.

[6] Jahn, A., H. Bischl, G. Heib, "Channel Characterization for Spread Spectrum Satellite Communication," IEEE 4th International Symposium on Spread Spectrum Techniques and Applications Proceedings, Volume 3, September 22-25, 1996, pp. 1221-1226.

[7] Van Dierendonck, A. J., *GPS Receivers*, Chapter 8, Vol. I, Global Positioning System: Theory and Applications, AIAA, Washington, D. C., 1996.

[8] Van Dierendonck, A. J., P. Fenton, T. Ford, "Theory and Performance of Narrow Correlator Spacing in a GPS Receiver," pp. 265-283 , NAVIGATION, J. of the ION, Vol. 39, No. 3, Fall 1992.

[9] Hegarty, C., "Derivation of the Discrimination Function with and without Multipath for the Non-Coherent Dot-Product Discriminator," MITRE White Paper, November 30, 2009.

[10] Jones, C. S., J. M. Finn, and N. Hengartner, "Regression with Strongly Correlated Data," Los Alamos National Laboratory, Los Alamos, NM, September 1, 2006.

[11] Forssell, B., *Radio Navigation Systems*, Section 2.3, Prentice Hall, New York, NY, 1991.

[12] Brenner, M., R. Reuter, and B. Schipper, "GPS Landing System Multipath Evaluation Techniques and Results," *Proceedings of The Institute of Navigation ION GPS-98*, Nashville, Tennessee, September 1998.

[13] Navstar GPS Space Segment/User Segment L1C Interfaces, Interface Specification, Draft IS-GPS-800, System Program Director, GPS Joint Program Office, April 19, 2006.

[14] Global Positioning System, Standard Positioning Service, Performance Standard, DOD, USA, 4th Edition, September 2008.

[15] Navstar GPS Space Segment/Navigation User Interfaces, Interface Specification, IS-

GPS-200D, March 7, 2006.

[16] http://sedac.ciesin.columbia.edu/gpw/

[17] Galileo Open Service SIS ICD Draft 1, February 2008

[18] A. Aragón, R. Orús, F. Amarillo, M. Hernández-Pajares, J.M. Juan, J. Sanz, "Preliminary NeQuick assessment for future single frequency users of GALILEO", 6thGeomatic Week, 8th-11th February 2005, Barcelona

[19] Avila-Rodriguez J.-A., Hein G.W., Wallner S., Schueler T., Schueler E., Irsigler M., "Revised Combined Galileo/GPS Frequency and Signal Performance Analysis", Proceedings of the ITM of the Institute of Navigation, ION-GNSS 2005, 13-16 September, 2005, Long Beach, California